

## COSMOLOGICAL CONSTRAINTS FROM GRAVITATIONAL LENS TIME DELAYS

DAN COE AND LEONIDAS A. MOUSTAKAS

Jet Propulsion Laboratory, California Institute of Technology, 4800 Oak Grove Dr, MS 169-327, Pasadena, CA 91109  
*Accepted for Publication in the Astrophysical Journal*

### ABSTRACT

Future large ensembles of time delay lenses have the potential to provide interesting cosmological constraints complementary to those of other methods. In a flat universe with constant  $w$  including a Planck prior, LSST time delay measurements for  $\sim 4,000$  lenses should constrain the local Hubble constant  $h$  to  $\sim 0.007$  ( $\sim 1\%$ ),  $\Omega_{de}$  to  $\sim 0.005$ , and  $w$  to  $\sim 0.026$  (all  $1\text{-}\sigma$  precisions). Similar constraints could be obtained by a dedicated gravitational lens observatory (OMEGA) which would obtain precise time delay and mass model measurements for  $\sim 100$  well-studied lenses. We compare these constraints (as well as those for a more general cosmology) to the “optimistic Stage IV” constraints expected from weak lensing, supernovae, baryon acoustic oscillations, and cluster counts, as calculated by the Dark Energy Task Force. Time delays yield a modest constraint on a time-varying  $w(z)$ , with the best constraint on  $w(z)$  at the “pivot redshift” of  $z \approx 0.31$ . Our Fisher matrix calculation is provided to allow time delay constraints to be easily compared to and combined with constraints from other experiments. We also show how cosmological constraining power varies as a function of numbers of lenses, lens model uncertainty, time delay precision, redshift precision, and the ratio of four-image to two-image lenses.

*Subject headings:* cosmological parameters – dark matter — distance scale — galaxies: halos — gravitational lensing — quasars: general

### 1. INTRODUCTION

The HST Key Project relied on 40 Cepheids to constrain Hubble’s constant  $H_0$  to 11% (Freedman et al. 2001). The first convincing measurements of the accelerating expansion rate of the universe (suggesting the existence of dark energy) by Riess et al. (1998) and Perlmutter et al. (1999) required 50 and 60 supernovae, respectively. So far, time delays have only been reliably measured for  $\sim 16$  gravitational lenses, thanks to dedicated lens monitoring from campaigns such as COSMOGRAIL (Eigenbrod et al. 2005). Yet recent analyses of 10–16 time delay lenses already claim to match or surpass the Key Project’s 11% precision on  $H_0$  (Saha et al. 2006; Oguri 2007; Coles 2008). Future surveys promise to yield hundreds or even thousands of lenses with well-measured time delays, which will enable us to obtain much tighter constraints on  $H_0$  as well as constraints on other cosmological parameters.

To date, most efforts have focused on studies of individual time delay lenses. In theory, one might be able to control all systematics and constrain  $H_0$  unambiguously given a single “golden lens”. Such a lens would have a sufficiently simple and well-measured geometry. The closest to a golden lens may be B1608+656. In Suyu et al. (2009b), the authors claim all systematics have been controlled to 5%. A new estimate for  $H_0$  based on this lens is forthcoming (Suyu et al. 2009a).

Historically, analyses of individual lenses have yielded varying answers for  $H_0$  (see the Appendix of Jackson 2007 for a recent review). This can be attributed to two factors, both of which, it appears, are now being overcome.

The first factor is simple intrinsic variation in lens properties (especially mass slope) and environment (lensing contributions from neighboring galaxies). Consider

the following estimate from a simple empirical argument. If statistical uncertainties on  $H_0$  decrease as  $1/\sqrt{N}$  (assuming systematics can be controlled), and the current uncertainty from 16 lenses is  $\sim 10\%$ , then the uncertainty on a single lens might be  $\sim 40\%$ . Thus, assuming  $h = 0.7$  (where  $H_0 = 100h \text{ km s}^{-1} \text{ Mpc}^{-1}$ ), individual lenses may be expected to yield a wide range of  $h = 0.42 - 0.98$  ( $1\text{-}\sigma$ ). (We will revisit these assumptions in this work.)

The second factor in the wide range of reported  $H_0$  values is that different analyses have assumed different mass profiles to model the lenses, including isothermal, de Vaucouleurs, and mass follows light. There is substantial weight of evidence that galaxy lenses are roughly isothermal on average, at least within approximately the scale radius (e.g., Koopmans et al. 2006). Theoretical work supports this idea, showing that a wide range of plausible luminous plus dark matter profiles all combine to yield roughly an isothermal profile *at the Einstein radius*, though the slope may deviate from isothermal beyond that radius (van de Ven et al. 2009).

In recent years we have witnessed a steady increase in the number of strong lenses discovered by searches such as CLASS (Myers et al. 2003), SLACS (Bolton et al. 2006), SL2S (Cabanac et al. 2007), SLS (Inada et al. 2008), HAGGLEs (Marshall et al. 2009b), and searches of AEGIS (Moustakas et al. 2007) and COSMOS (Faure et al. 2008). Based on this experience, we can expect that future surveys such as Pan-STARRS<sup>1</sup> (Kaiser 2004), LSST<sup>2</sup> (Ivezic et al.

<sup>1</sup> The Panoramic Survey Telescope & Rapid Response System, <http://pan-starrs.ifa.hawaii.edu>

<sup>2</sup> The Large Synoptic Survey Telescope, <http://www.lsst.org>

2008), JDEM / IDECS<sup>3</sup>, and SKA<sup>4</sup> (Lazio 2008) will yield an explosion in the number of strong lenses known (e.g., Koopmans et al. 2004; Fassnacht et al. 2004; Marshall et al. 2005). Prospects for using these lenses to constrain the nature of dark matter over the course of the next decade were presented in Moustakas et al. (2009), Koopmans et al. (2009a), and Marshall et al. (2009a).

It is reasonable to expect that time delays will be reliably measured for large numbers of these lenses, whether through repeated observations in surveys (Pan-STARRS and LSST), auxiliary monitoring, and/or through tailored specific missions such as OMEGA (Moustakas et al. 2008). Increased sample size, improved lens model constraints, and higher precision redshifts and time delay measurements will all improve constraints on  $H_0$  and other cosmological parameters, as we present below.

A more precise measurement of  $H_0$  will yield tighter constraints on both the dark energy equation of state parameter ( $w$ ) and the flatness of our universe ( $\Omega_k$ ), independently of the results of future dark energy surveys (Blake et al. 2004; Hu 2005; Albrecht et al. 2006; Olling 2007). To this end, the SHOES Program (Supernovae and  $H_0$  for the Equation of State) has obtained new observations of supernovae and Cepheid variables with reduced systematics. Recently, Riess et al. (2009) published a redetermination of  $H_0 = 74.2 \pm 3.6 \text{ km s}^{-1} \text{ Mpc}^{-1}$ , or 5% uncertainty including both statistical and systematic errors. Their  $H_0$  determination plus WMAP 5-year data alone constrain  $w = -1.12 \pm 0.12$  (assuming constant  $w$ ).

Riess et al. (2009) also make the following important point that bears repeating. The seemingly tight constraints on  $H_0$  derived from CMB + BAO + SN experiments are in fact *predictions* or *inferences* of  $H_0$  given those data and a cosmological model. They are no substitute for direct measurement of  $H_0$  such as that presented in their work or the HST Key Project.

Olling (2007) reviews several methods with the potential to directly constrain  $H_0$ . Water masers, for example, hold much promise (Braatz et al. 2008; Braatz 2009). Time delays and water masers both yield direct geometric measurements of the universe to the redshifts of the observed sources ( $z \sim 2$  or greater for time delay lenses), bypassing all distance ladders.

Time delays do not simply constrain  $H_0$ . To first order, each time delay is proportional to the angular diameter distance to the lensed object and thus inversely proportional to  $H_0$ . An additional factor involves a ratio of two other distances – from observer to lens and from lens to source. All three of these distances have a complex (though weaker) dependence on the other cosmological parameters ( $\Omega_m, \Omega_{de}, \Omega_k, w_0, w_a$ ) which contribute to the expansion history of the universe.

Most time delay analyses ignore this weaker dependence on ( $\Omega_m, \Omega_{de}, \Omega_k, w_0, w_a$ ), in effect assuming these parameters are known perfectly. In this paper we show how relaxing this “perfect prior” increases the uncertainties on  $H_0$ . As dark energy surveys endeavor to place constraints on  $w$  and the flatness of our universe  $\Omega_k$ , we must

study how time delays can contribute to these constraints without assuming the very parameters we would like to constrain. In this work we also study the ability of large time delay ensembles to constrain ( $\Omega_m, \Omega_{de}, \Omega_k, w_0, w_a$ ).

The idea to use time delay lenses to measure  $H_0$  was first proposed by Refsdal (1964). Strong gravitational lenses are elegant geometric consequences of how light travels through the universe while grazing massive galaxies. When the line of sight alignment is very close, light takes multiple paths around the curved space of the lens. These paths form multiple images, and the light takes a different amount of time to travel each path. Light passing closer to the lens is deflected by a larger angle (increasing its path length) and experiences a greater relativistic time dilation, further delaying its arrival. If the source flares up, or otherwise varies in intensity (e.g., if it is an active galactic nucleus, or AGN), we can observe these “time delays” between or among the images. These time delays are functions of the angular diameter distances between the source, lens, and observer, as well as the properties of the lens itself.

The ability of time delays to constrain other cosmological parameters has also been explored. Lewis & Ibata (2002) explored various combinations of ( $\Omega_m, \Omega_\Lambda$ ) in a flat universe and various ( $w_0, w_a$ ) for fixed ( $\Omega_m, \Omega_{de}$ ). Most notably, they calculated constraints on ( $h, w$ ) from ensembles of lenses assuming constant  $w$  and ( $\Omega_m, \Omega_\Lambda$ ) = (0.3, 0.7), finding that  $h$  and  $w$  would not be strongly constrained. We show that the addition of a Planck prior improves these constraints considerably. Linder (2004) investigated constraints on the dark energy parameters ( $w_0, w_a$ ) from various methods, touting the complementarity of strong lensing to that of other methods. However, they concede that the unique positive correlation in strong lensing ( $w_0, w_a$ ) constraints evaporates when including degeneracies other cosmological parameters. Mörtzell & Sunesson (2006) and Dobke et al. (2009) examined the constraints that large ensembles of lenses might place on  $H_0$  and  $\Omega_\Lambda = 1 - \Omega_m$  (assuming a flat universe). Below we present the first full treatment of the cosmological constraints expected on ( $h, \Omega_m, \Omega_{de}, \Omega_k, w_0, w_a$ ) from ensembles of time delay lenses including various priors.

Lens statistics from well-controlled searches for strongly-lensed sources have also been used to constrain cosmology (e.g., Chae 2007; Oguri et al. 2008). If time delays can be obtained for the lenses in such a sample, the lens statistics and time delays might combine to yield tighter cosmological constraints. This potential is not explored in this work.

Cosmological constraints can also be obtained from symmetric strong lenses for which velocity dispersions have been measured (e.g., Paczynski & Gorski 1981; Futamase & Hamaya 1999; Yamamoto et al. 2001; Lee & Ng 2007). Assuming an isothermal model, the measured velocity dispersion determines the Einstein radius solely as a function of cosmology (given redshifts measured to the lens and source). Yamamoto et al. (2001) studied the future potential for this method to constrain cosmology using a Fisher matrix analysis.

The reader is invited to skip ahead to our results in §5, where cosmological constraints expected from time delays (according to our calculations) are compared to those expected from other methods (weak lensing, super-

<sup>3</sup> The Joint Dark Energy Mission, <http://jdem.gsfc.nasa.gov>

<sup>4</sup> The Square Kilometer Array, <http://www.skatelescope.org>

novae, baryon acoustic oscillations, and cluster counts). Table 2 summarizes the assumed priors including a guide to specific sections and figures.

The remainder of our paper is organized as follows. In §2 we provide the time delay equations and discuss how cosmology is derived from observed time delays. We define the quantity  $\mathcal{T}_C(h, \Omega_m, \Omega_{de}, \Omega_k, w_0, w_a; z_L, z_S)$  which time delays are capable of constraining. In §3 we estimate the constraints on  $\mathcal{T}_C$  expected from future experiments. (A more detailed analysis of lensing simulations is presented in a companion paper Coe & Moustakas 2009a, hereafter Paper I.) In §4 we illustrate the dependence of  $\mathcal{T}_C$  on cosmological parameters  $(h, \Omega_m, \Omega_{de}, w_0, w_a)$ . In §5, as highlighted above, we give projections for time delay constraints on  $(h, \Omega_{de}, \Omega_k, w_0, w_a)$  and compare to other methods. Systematic biases are discussed in §6 and their impact on our ability to constrain cosmology is analyzed in another companion paper (Coe & Moustakas 2009c, hereafter Paper III). Finally we present our conclusions in §7.

We assume all constraints to be centered on the concordance cosmology  $h = 0.7$ ,  $\Omega_m = 0.3$ ,  $\Omega_{de} = 0.7$ ,  $\Omega_k = 0$ ,  $w_0 = -1$ , and  $w_a = 0$ , where  $H_0 = 100h \text{ km s}^{-1} \text{ Mpc}^{-1}$ .

## 2. COSMOLOGICAL CONSTRAINTS FROM TIME DELAYS

### 2.1. Time Delay Equations

A galaxy at redshift  $z_L$  strongly lenses a background galaxy at redshift  $z_S$  to produce multiple images. Either two or four images are typically produced.<sup>5</sup> We refer to these cases as “doubles” and “quads”, respectively. The lensing effect delays each image in reaching our telescope by a different amount of time, given by

$$\Delta\tau = \frac{(1+z_L)}{c} \mathcal{D} \left[ \frac{1}{2} |\boldsymbol{\theta} - \boldsymbol{\beta}|^2 - \phi \right] \quad (1)$$

(e.g., Blandford & Narayan 1986) with terms defined below. The factors in the time delay equation can be grouped into a product of two terms:

$$\Delta\tau = \mathcal{T}_C \mathcal{T}_L. \quad (2)$$

The first factor,

$$\mathcal{T}_C \equiv \frac{(1+z_L)}{c} \mathcal{D}, \quad (3)$$

is a function of cosmology and the lens and source redshifts,  $z_L$  and  $z_S$ . The second factor,

$$\mathcal{T}_L \equiv \left[ \frac{1}{2} |\boldsymbol{\theta} - \boldsymbol{\beta}|^2 - \phi \right], \quad (4)$$

is a function of the projected lens potential  $\phi$ , the source galaxy’s position on the sky  $\boldsymbol{\beta}$ , and the image positions  $\boldsymbol{\theta}$ .

We concentrate on the cosmological dependence of  $\mathcal{T}_C$ . The factor

$$\mathcal{D} \equiv \frac{D_L D_S}{D_{LS}} \quad (5)$$

<sup>5</sup> An additional central demagnified image is also produced by every lens with a central mass profile shallower than isothermal. Such images are rarely bright enough to be detected, thus we ignore them throughout this work.

is a ratio of the angular-diameter distances from observer to lens  $D_L = D_A(0, z_L)$ , observer to source  $D_S = D_A(0, z_S)$ , and lens to source  $D_{LS} = D_A(z_L, z_S)$ . Angular-diameter distances are calculated as follows (Fukugita et al. 1992, filled beam approximation; see also Hogg 1999):

$$D_A(z_1, z_2) = \frac{c}{H_0} \frac{E_A(z_1, z_2)}{1+z_2}, \quad (6)$$

$$E_A = \frac{\text{sinn} \left[ \sqrt{|\Omega_k|} E_A^* \right]}{\sqrt{|\Omega_k|}}, \quad (7)$$

where  $\text{sinn}(u) = \sin(u)$ ,  $u$ , or  $\sinh(u)$  for an open, flat, or closed universe respectively ( $\Omega_k < 0$ ,  $\Omega_k = 0$ , or  $\Omega_k > 0$ ). The curvature is given by  $\Omega_k \equiv 1 - (\Omega_m + \Omega_\Lambda)$ , while

$$E_A^*(z_1, z_2) = \int_{z_1}^{z_2} \frac{dz'}{E(z')}. \quad (8)$$

The normalized Hubble parameter  $E(z)$  can have different expressions depending on the cosmology assumed:

$$\begin{aligned} E(z) &\equiv \frac{H(z)}{H_0} \\ &= \sqrt{\Omega_m(1+z)^3 + \Omega_k(1+z)^2 + \Omega_\Lambda} \\ &= \sqrt{\Omega_m(1+z)^3 + \Omega_k(1+z)^2 + \Omega_{de}(1+z)^{3(1+w)}} \\ &= \sqrt{\dots + \Omega_{de}(1+z)^{3(1+w_0+w_a)} \exp\left(\frac{-3w_a z}{1+z}\right)}. \end{aligned} \quad (9)$$

Here we have progressed from a universe with a cosmological constant  $\Omega_\Lambda$  to one with dark energy with an equation of state  $p = w\rho$ . In the last line, the last term has been rewritten in terms of an evolving dark energy equation of state

$$w = w_0 + w_a(1-a) \quad (10)$$

$$= w_0 + w_a \left( \frac{z}{1+z} \right), \quad (11)$$

a common parametrization first introduced by Chevallier & Polarski (2001) and Linder (2003). The universe scale factor  $a = (1+z)^{-1}$ .

We next define the dimensionless ratio

$$\mathcal{E} \equiv \frac{E_L E_S}{E_{LS}} \quad (12)$$

with factors defined similarly to those above for  $D_A$ :  $E_L = E_A(0, z_L)$ ,  $E_S = E_A(0, z_S)$ ,  $E_{LS} = E_A(z_L, z_S)$ . We find that many factors cancel, and  $\mathcal{T}_C$  simplifies to:

$$\mathcal{T}_C = \frac{\mathcal{E}(\Omega_m, \Omega_{de}, \Omega_k, w_0, w_a)}{H_0}. \quad (13)$$

We see here clearly that time delays ( $\Delta\tau = \mathcal{T}_C \mathcal{T}_L$ ) scale

inversely with  $H_0$ . There is also a complex though weaker dependence on the other cosmological parameters as embedded in  $\mathcal{E}$ .

### 2.2. Deriving Cosmology from Time Delays

Given observed time delays  $\Delta\tau$  and assuming a lens model (and thus  $\mathcal{T}_{\mathcal{L}}$ ), one can obtain measures of  $\mathcal{T}_{\mathcal{C}}$ . These measures will have some scatter due to both observational uncertainties and deviations of the lens from the assumed model.

Recent studies suggest that galaxy lenses, on average, have roughly isothermal profiles within the Einstein radius (see §1). Deviations from this simple description include variation in lens slope, external shear, mass sheets, and substructure. Oguri (2007) parametrized the deviations as the “reduced time delay”, the ratio of the observed time delay to that expected due to an isothermal potential in a given lens:

$$\Xi \equiv \frac{\Delta\tau}{\Delta\tau_{\text{iso}}}. \quad (14)$$

In our notation, these observed deviations are due to deviations in the lens model:

$$\Xi_{\mathcal{L}} \equiv \frac{\mathcal{T}_{\mathcal{L}}}{\mathcal{T}_{\mathcal{L},\text{iso}}}. \quad (15)$$

By assuming an isothermal model ( $\mathcal{T}_{\mathcal{L}} = \mathcal{T}_{\mathcal{L},\text{iso}}$ ), these deviations get absorbed into the derived cosmology:

$$\Xi_{\mathcal{C}} \equiv \frac{\mathcal{T}_{\mathcal{C}}}{\mathcal{T}_{\mathcal{C},\text{true}}}, \quad (16)$$

where  $\mathcal{T}_{\mathcal{C},\text{true}}$  is the true cosmology. For example, a lens which is steeper than isothermal yields  $\Xi_{\mathcal{L}} > 1$ ; thus when assuming an isothermal model ( $\Xi_{\mathcal{L}} = 1$ ), we derive  $\Xi_{\mathcal{C}} > 1$  (since  $\Xi = \Xi_{\mathcal{C}}\Xi_{\mathcal{L}}$ ). In traditional analyses assuming fixed  $\mathcal{E}$ ,  $\Xi_{\mathcal{C}} > 1$  would simply yield a low  $h$ . This approximation is adequate for small samples of lenses but not for the large samples to come in the near future (§5.4.1).

Similarly, observational uncertainties affecting  $\Delta\tau$  are absorbed into the derived cosmology. In this paper, we study how observational and intrinsic (lens model) uncertainties combine to yield scatter in the observed  $\Delta\tau$ . We will assume these measurements yield  $\mathcal{T}_{\mathcal{C}}$  with the correct mean but a simple Gaussian scatter and explore how this propagates to Gaussian uncertainties on cosmological parameters.

In practice we do not expect  $\Xi_{\mathcal{L}}$  and measurements of  $\Delta\tau$  to have Gaussian scatter, but these serve as useful approximations. The true expected  $P(\Xi)$  from time delay measurements and methods for handling these distributions are studied in Oguri (2007) and Paper I.

## 3. CONSTRAINTS ON $\mathcal{T}_{\mathcal{C}}$ FROM FUTURE EXPERIMENTS

### 3.1. Extrapolating from Current Empirical Results

Recent studies have constrained  $\mathcal{T}_{\mathcal{C}}$  to  $\sim 10\%$  using time delays, where  $\mathcal{T}_{\mathcal{C}}$  encodes all of the cosmological dependencies (§2.1). Constraints on  $\mathcal{T}_{\mathcal{C}}$  have generally been interpreted to be equivalent to direct constraints on  $h$ . This assumption is reasonable for current sample sizes,

but will need to be revised in the future (§5.4.1). Using 16 lenses, Oguri (2007) obtain  $h = 0.70 \pm 0.06(\text{stat.})$ . Similar studies by Saha et al. (2006) and Coles (2008) using a different method obtain similar constraints using 10 and 11 lenses, respectively. The latter finds  $h = 0.71^{+0.06}_{-0.08}$ .

We will adopt the Oguri (2007) uncertainty of 8.6% with 16 lenses as the “current” uncertainty in  $\mathcal{T}_{\mathcal{C}}$ .<sup>6</sup> We note that the time delay uncertainties in this sample are roughly and broadly scattered about  $\Delta(\Delta\tau) = 2$  days.<sup>7</sup>

We can improve on these  $\mathcal{T}_{\mathcal{C}}$  constraints in three ways: obtaining larger samples of lenses, better constraining our lens models, and obtaining more precise time delay measurements. As we explain below, we expect future surveys such as Pan-STARRS and LSST to improve on the sample size while the lens model and time delay uncertainties will remain about the same. These surveys will have to contend with a lack of spectroscopic redshifts for most objects, but the gains in sample size will more than compensate. Similarly tight constraints on  $\mathcal{T}_{\mathcal{C}}$  could also be obtained by studying relatively fewer lenses in great detail, as we discuss below.

Here we consider statistical uncertainties only, with systematics to be discussed in §6. We will assume that all other things being equal, increasing our sample size beats down our errors by  $\sqrt{N}$  for  $N$  lenses. This assumption is borne out well by our detailed simulations (Paper I), for the case of no systematic uncertainties.

Based on the current constraint of  $\delta\mathcal{T}_{\mathcal{C}} \approx 8.6\%$  from 16 lenses (Oguri 2007), we project that simply increasing the sample of lenses would produce constraints of  $\delta\mathcal{T}_{\mathcal{C}} \approx 34\%/\sqrt{N}$ . We will define this as the uncertainty from lens models and time delay measurements:  $\delta\Xi_{\mathcal{L}\tau} \sim 0.344$ . Photometric redshifts would degrade these constraints as estimated below (§3.3).

### 3.2. Future Surveys

Pan-STARRS and LSST will both survey the sky repeatedly, opening the time domain window for astronomical study over vast solid angles. Pan-STARRS 1 (PS1) has recently begun its  $3\pi$  survey, repeatedly observing the entire visible sky to  $\sim 23$ rd magnitude every week over a 3-year period. LSST promises similar coverage and depth every 3 nights with first light scheduled for 2014.

These surveys will reveal many time-variable sources, among them gravitationally-lensed quasars. The persistent monitoring over many years should yield time delays “for free” for many strongly-lensed quasars. Simulations (M. Oguri 2009, private communication) show that Pan-STARRS 1 and LSST are expected to yield  $\sim 1,000$  and  $\sim 4,000$  strongly-lensed quasars with quad fractions of 19% and 14%, respectively.

We will assume that these surveys will measure time delays to about 2-day precision, or similar to that of

<sup>6</sup> The Oguri (2007) simulations initially suggested an uncertainty of  $\sim 4\%$  in  $\mathcal{T}_{\mathcal{C}}$ . However jackknife resampling of the data revealed the true uncertainty to be twice as much. Under-prescribed shear in the simulations was cited as a potential cause for the discrepancy.

<sup>7</sup> We adopt a notation in which “ $\Delta$ ” refers to uncertainties with units and “ $\delta$ ” to fractional uncertainties. Thus a time delay of 20 days measured to 2-day precision has  $\Delta(\Delta\tau) = 2$  days and  $\delta(\Delta\tau) = 0.1$ .

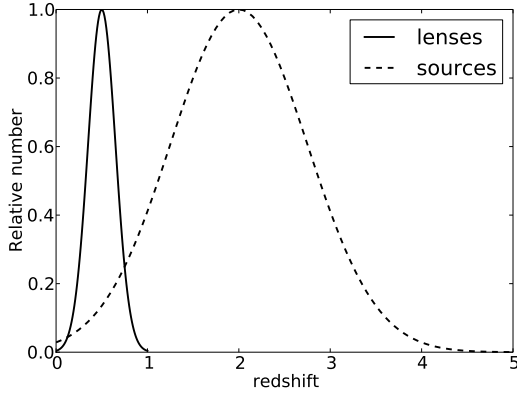


FIG. 1.— Distributions of lens and source redshifts used in this paper. These Gaussian distributions ( $z_L = 0.5 \pm 0.15$ ,  $z_S = 2.0 \pm 0.75$ ;  $z_S > z_L$ ) were used by Dobke et al. (2009) as reasonable approximations for near-future missions including LSST.

our current sample of time delay lenses. This is consistent with predictions based on detailed simulations by Eigenbrod et al. (2005) which study factors including survey cadence, object visibility, and the complicating effects of microlensing. We note this estimate may be a bit optimistic for PS1 with its slower sampling rate compared to LSST.

The expected redshift distributions of the lenses and sources can be roughly approximated by the Gaussian distributions  $z_L = 0.5 \pm 0.15$  and  $z_S = 2.0 \pm 0.75$  with  $z_S > z_L$  (Fig. 1), as adopted by Dobke et al. (2009). Obviously the two distributions will be correlated, but we approximate them as being independent.

As surveys attain fainter magnitude limits, it is believed that the magnification bias enjoyed by quads will be diminished. Future surveys are thus expected to yield lower quad fractions ( $\sim 19\%$ ,  $14\%$ ) than the current sample of time delay lenses ( $6 / 16 = 37.5\%$ ). This might improve the expected constraints on  $\mathcal{T}_C$  from future surveys as quads have been shown to yield time delays with more scatter and thus less reliable estimates of  $\mathcal{T}_C$  (Oguri 2007, Paper I).<sup>8</sup> However, we find this to be mitigated by the fact that quads yield multiple time delay measurements (one for each pair of images), while doubles only yield a single  $\Delta\tau$  measurement. Based on our detailed simulations and analysis (Paper I), we find quads and doubles to have approximately equal power to constrain  $\mathcal{T}_C$ . This simplifies our analysis; the quad-to-double ratio need not be considered when estimating  $\delta\mathcal{T}_C$  for a given experiment. To allay any concern, we stress that this assumption actually makes our estimates of  $\delta\mathcal{T}_C$  more conservative for future surveys which have lower quad fractions than the current sample.

For each double or quad, image pairs can be further classified by their geometry. For example, image pairs with small opening angles are found to yield larger scatter in  $\Delta\tau$  (Oguri 2007, Paper I). Detailed analyses in these papers quantify these scatters, enabling a well-informed prior  $P(\Xi)$  to be placed on each image pair as a function of geometry. The details are unimportant here

<sup>8</sup> This is believed to be due to the fact that some of the factors (especially external shear) which cause scatter in  $\Xi$  also raise the likelihood that a lens will produce quad images rather than a double.

though we have made use of the constraint this analysis has put on  $\mathcal{T}_C$  (Oguri 2007).

### 3.3. Photometric Redshift Uncertainties

Currently all lenses which have reliable time delay measurements also have spectroscopic redshifts measured for both lenses and sources (e.g., Oguri 2007). The telescope time required to obtain spectroscopic redshifts is generally a small fraction of that required to obtain accurate time delays, so the extra investment is worthwhile.

Future surveys which repeatedly scan the sky, however, will yield time delays for many more lenses than may be followed up spectroscopically. For these lenses we will have to rely on photometric redshift measurements. These uncertainties will degrade the constraints possible on the cosmological parameters.

Photometric redshift uncertainties for the lenses (typically elliptical galaxies at  $z_L \sim 0.5$ ) are expected to be  $\Delta z_L \sim 0.04(1 + z_L)$ , similar to that found in the CFHT Legacy Survey (Ilbert et al. 2006). Redshift uncertainties for the lensed sources (quasars) are expected to be somewhat higher. We will adopt  $\Delta z_S \sim 0.10(1 + z_S)$ , roughly that found in the analysis of  $\sim$ one million SDSS quasars (Richards et al. 2009).

Obtaining photometric redshifts in ground-based images will often be complicated by cross-contamination of flux among the lens and multiple images. Yet improved photometric redshift techniques are also being developed with LSST in mind (Schmidt et al. 2009), so it is perhaps too early to say whether our estimated redshift uncertainties are too optimistic or pessimistic for a future ground-based survey. Some of the most common catastrophic redshift degeneracies can clearly be avoided by considering the observed image separations, time delays, etc. Most obviously, the common degeneracy between  $z \sim 0.2$  and  $z \sim 3$  (e.g., Coe et al. 2006) can be neatly averted since a lens at  $z \sim 3$  or a source at  $z \sim 0.2$  would clearly stand out.

Assuming the above redshift uncertainties, we now determine how these propagate into uncertainties on  $\mathcal{T}_C$ . For simplicity, let us assume that redshift uncertainties are Gaussian. Let us further assume that uncertainty in  $\Xi$  scales linearly with redshift uncertainty. (This is approximately true for reasonable uncertainty levels  $\Delta z \lesssim 0.2$ .)

Using equations 7 – 13, we find for a typical lens-source combination with  $(z_L, z_S) = (0.5, 2.0)$ , that lens and source redshift uncertainties translate to  $\delta\Xi_{z_L} \sim 2.75\Delta z_L$  and  $\delta\Xi_{z_S} \sim -0.16\Delta z_S$ , respectively. Given the above redshift uncertainties, these evaluate to  $\delta\Xi_{z_L} \sim 0.16$  and  $\delta\Xi_{z_S} \sim 0.05$ . These relations are strong functions of redshift and become catastrophic for sources very close to the lens. We plot this behavior in Fig. 2. If accurate and precise redshifts are not available, we must concentrate our analysis on systems with high separation in redshift between the lens and source.

For a lens ensemble with Gaussian redshift distributions  $z_L = 0.5 \pm 0.15$  and  $z_S = 2.0 \pm 0.75$ , we find  $\delta\Xi_{z_L} \sim 0.175$  and  $\delta\Xi_{z_S} \sim 0.028$ . To calculate these uncertainties, we sum the  $\chi^2$  of individual lens-source combinations, weighting by the probability  $P_i$  of observing that combination:

$$\frac{1}{\sigma^2} = \sum_i \frac{P_i}{\sigma_i^2}. \quad (17)$$

Note that this sum naturally assigns more weight to more confident measurements.

Assuming the lens and source redshift uncertainties can be added in quadrature,

$$\delta\Xi_{\mathcal{Z}}^2 = \delta\Xi_{\mathcal{Z}_L}^2 + \delta\Xi_{\mathcal{Z}_S}^2, \quad (18)$$

we find  $\delta\Xi_{\mathcal{Z}} \sim 0.177$ .

Of course, these are just estimates for large ensembles. In practice, redshift probability distributions  $P(z)$  for individual galaxies will be properly folded into the  $P(\mathcal{T}_C)$  determinations. Biased redshifts would yield biased  $\mathcal{T}_C$ , the effects of which we study in Paper III.

### 3.4. Projected Constraints from Large Surveys

We now calculate the total uncertainty  $\delta\mathcal{T}_C$  expected for large surveys with photometric redshifts. The combined lens model and time delay uncertainties are  $\delta\Xi_{\mathcal{L}\tau} \sim 0.344$ , based on extrapolation of the current empirical Oguri (2007) finding (§3.1). We estimate uncertainties of  $\delta\Xi_{\mathcal{Z}} \sim 0.177$  due to redshift uncertainties of  $\Delta z_L \sim 0.04(1 + z_L)$  and  $\Delta z_S \sim 0.10(1 + z_S)$  for the lenses and sources, respectively (§3.3).

The simplest estimate of the total uncertainty is to add these uncertainties in quadrature:

$$\delta\Xi^2 = \delta\Xi_{\mathcal{L}\tau}^2 + \delta\Xi_{\mathcal{Z}}^2. \quad (19)$$

This yields  $\delta\Xi \sim 0.387$ .

To be more precise, all of the uncertainties should be added in quadrature for each lens individually before combining them according to Eq. 17. Repeating the analysis in this way, we find  $\delta\Xi \sim 0.402$ .

Thus we expect large surveys with photometric uncertainties given above to yield  $\delta\mathcal{T}_C \sim 40\%/\sqrt{N}$ . We project  $\delta\mathcal{T}_C \sim 1.3\%$  for PS1 (1,000 lenses) and  $\delta\mathcal{T}_C \sim 0.64\%$  for LSST (4,000 lenses).

Table 1 summarizes the progress we can expect to make in “Stages” corresponding to those defined by the Dark Energy Task Force (DETF; Albrecht et al. 2006, 2009): “Stage I” = current, “II” = ongoing, “III” = currently proposed, “IV” = large new mission. Again, we stress these are estimates of statistical uncertainties only. Large surveys are compared to dedicated monitoring and detailed analysis of a smaller sample of lenses.

We might have made our analysis more sophisticated still, calculating  $\delta\Xi_{\mathcal{L}\tau}$ ,  $\delta\Xi_{\mathcal{Z}_L}$ , and  $\delta\Xi_{\mathcal{Z}_S}$  individually for each lens-source combination in our ensemble. Lenses and sources at higher redshift, for example, will be brighter and higher magnification cases on average, altering their  $\delta\Xi_{\mathcal{L}\tau}$  somewhat. The approximations made in our above analysis should suffice for our purposes here.

### 3.5. Quality vs. Quantity

Thus far we have assumed that detailed observations and analysis would not be performed on the lenses. The alternative is to study fewer lenses in more detail, reducing the uncertainties for each lens. In practice, we expect

both strategies to be pursued and the combined power of both analyses to place the tightest possible constraints on  $\mathcal{T}_C$ .

Moustakas et al. (2008) have designed a mission concept that would be dedicated to monitoring a sample of four-image lenses, with the primary goal of constraining fundamental properties of dark matter. This space-based Observatory for Multi-Epoch Gravitational Lens Astrophysics (OMEGA) would monitor 100 time delay lenses to achieve precise and accurate  $\lesssim 0.1$  day time delay measurements. Supporting measurements would aim to reduce the model uncertainty of each lens to 5% ( $\delta\Xi_{\mathcal{L}} = 0.05$ ) and thus constrain  $\mathcal{T}_C$  to 5% with each lens, as claimed recently for B1608+656 (Suyu et al. 2009a). These supporting measurements, including velocity dispersion in the lens and characterization of the group environment (see discussion in §6.2), would be carried out either with OMEGA itself or through coordinated efforts by ground-based telescopes and JWST. Spectroscopic redshifts would also be obtained for the 100 lens galaxies and lensed quasars.

Lenses targeted by OMEGA will be quads, enabling measurements of time delay *ratios* among the image pairs. This would provide constraints on the dark matter substructure mass function (Keeton & Moustakas 2009; Keeton 2009, Moustakas et al., in preparation).

Given lens models accurate to 5% for 100 galaxies, we might expect OMEGA to yield  $\delta\mathcal{T}_C \sim 5\%/\sqrt{100} = 0.5\%$ . The time delays would be measured with sufficient precision so as not to contribute significantly to the total uncertainty in  $\delta\mathcal{T}_C$ . The multiple time delay measurements per lens (quad) also help reduce this contribution. Based on the expected time delay distribution for a sample of quads (Paper I), we estimate that  $\Delta(\Delta\tau) = 0.1$ -day uncertainties would inflate the  $\mathcal{T}_C$  uncertainty only to  $\sim 0.515\%$ .

If both LSST and OMEGA obtain their measurements of  $\mathcal{T}_C$  free of significant systematics, their combined power could further reduce the uncertainty to  $\delta\mathcal{T}_C \sim 0.4\%$ .

## 4. DEPENDENCE OF $\mathcal{T}_C$ ON COSMOLOGY

We expect LSST time delay lenses to constrain  $\mathcal{T}_C$  to  $\sim 0.64\%$ . In this section we begin to explore how this “Stage IV” constraint translates to constraints on cosmological parameters. We study the dependence of  $\mathcal{T}_C$  on  $(h, \Omega_m, \Omega_{de}, \Omega_k, w_0, w_a)$  for several cosmologies as outlined in Table 2.

### 4.1. Flat universe with a cosmological constant ( $h, \Omega_\Lambda = 1 - \Omega_m$ )

First, we add a single free parameter  $\Omega_\Lambda$  (in addition to  $h$ ) in considering a flat universe with a cosmological constant ( $w = -1$ ). Given  $\delta\mathcal{T}_C = 0.64\%$  from an ensemble with *all* lenses at  $z_L = 0.5$  and *all* sources at  $z_S = 2.0$ , we would obtain confidence contours shown in Fig. 4.

The shape of these curves shifts somewhat as a function of  $z_L$  and  $z_S$ . Given an ensemble of lenses and sources with Gaussian redshift distributions  $z_L = 0.5 \pm 0.15$  and  $z_S = 2.0 \pm 0.75$  as discussed above, we begin to break the  $(h, \Omega_\Lambda)$  degeneracy (Table 5). Assuming a flat universe, Stage IV time delays could provide independent evidence for  $\Omega_\Lambda > 0$ . Whether this remains interesting by Stage IV remains to be seen. The constraints on  $h$  are certainly

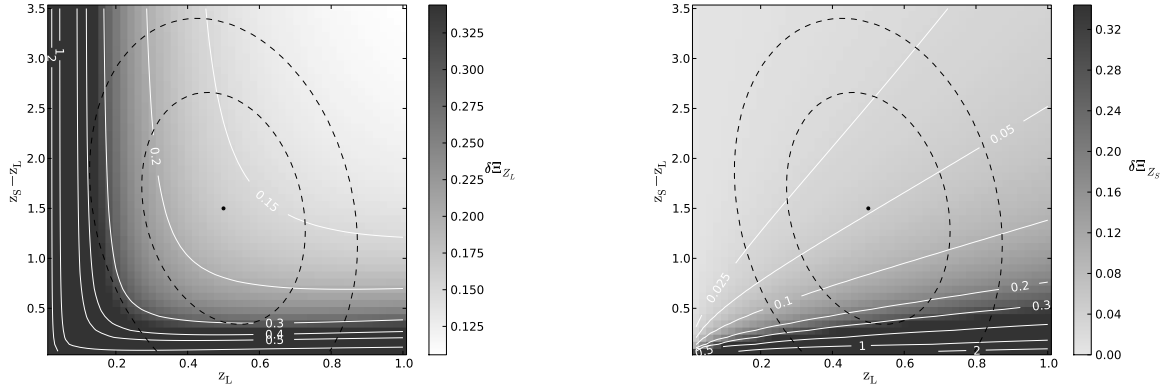


FIG. 2.— Photometric redshift uncertainties’ contributions to cosmological uncertainties in  $\mathcal{T}_C$ . *Left*: Uncertainty in  $\mathcal{T}_C$  (grayscale and contours) from lens redshift uncertainties of  $0.04(1 + z_L)$ , plotted as a function of lens redshift  $z_L$  and the lens-source redshift difference  $z_S - z_L$ . The dashed contours show the redshift distribution (1- and 2- $\sigma$  contours) assumed in this work. A dot at  $(z_L, z_S) = (0.5, 2.0)$  marks the center of the distributions. *Right*: Same for source redshift uncertainties of  $0.10(1 + z_L)$ . Note that the plots have different grayscales. For sources close to the lens (small  $z_S - z_L$ ), redshift uncertainties become catastrophic yielding large  $\delta\mathcal{T}_C$ . Lens redshift uncertainties are also problematic at low  $z_L$ .

TABLE 1  
ESTIMATED CURRENT AND FUTURE CONSTRAINTS ON  $\mathcal{T}_C$

Stage	Experiment	$N_L$	quads	$\Delta z^a$	$\Delta(\Delta\tau)$	$\delta\Xi_{\mathcal{L}}$	$\delta\mathcal{T}_C$
I	current	16	38%	spec	2 days	...	8.6%
II	Pan-STARRS 1	1,000	19%	phot	2 days	...	1.27%
IV	LSST	4,000	14%	phot	2 days	...	0.64%
IV	OMEGA	100	100%	spec	0.1 day	5%	0.5%
IV	LSST + OMEGA	...	...	...	...	...	0.4%

<sup>a</sup> Spectroscopic or photometric redshift measurements. For the latter we assume  $\Delta z_L = 0.04(1 + z_L)$  and  $\Delta z_S = 0.10(1 + z_S)$ .

TABLE 2  
COSMOLOGIES EXPLORED IN THIS WORK

Cosmology	$h$	$\Omega_m$	$\Omega_{de} / \Omega_{\Lambda}^a$	$\Omega_k$	$w_0$	$w_a$	Sections <sup>b</sup>	Figures
Flat universe with cosmological constant	Free	$1 - \Omega_{\Lambda}$	Free ( $\Omega_{\Lambda}$ )	0	-1	0	§4.1	4, 5
Curved universe with cosmological constant	Free	$1 - (\Omega_{\Lambda} + \Omega_k)$	Free ( $\Omega_{\Lambda}$ )	Free	-1	0	§4.2	6, 7
Flat universe with constant $w^c$	Free	$1 - \Omega_{de}$	Free	0	Free	0	§4.3, §5.2	8, 9, 12
Flat universe with time-variable $w$	Free	$1 - \Omega_{de}$	Free	0	Free	Free	§4.4	10
General (curved with time-variable $w$ ) <sup>d</sup>	Free	$1 - (\Omega_{de} + \Omega_k)$	Free	Free	Free	Free	§5.3	13, 14, 17

NOTE. — We consider six cosmological parameters of which five are independent since  $\Omega_m + \Omega_{de} + \Omega_k = 1$ .

<sup>a</sup> When  $w_0 = -1$  and  $w_a = 0$ ,  $\Omega_{de} = \Omega_{\Lambda}$ , the cosmological constant.

<sup>b</sup> In §4 the  $\mathcal{T}_C$  dependencies are explored. In §5 additional priors are assumed and time delay constraints are compared to those from other methods.

<sup>c</sup> Given this cosmology, we assume a Planck prior in §5.2.

<sup>d</sup> Given a general cosmology, in §5.3 we assume a prior of Planck + “Stage II” WL+SN+CL (see that section for details).

tighter and would be improved by the introduction of a prior on  $\Omega_{\Lambda}$ , which we defer until §5.

#### 4.2. Curved universe with cosmological constant ( $h, \Omega_m, \Omega_{\Lambda}, \Omega_k$ )

If we relax the flatness parameter, adding another free parameter  $\Omega_m$  (where curvature is determined by  $\Omega_k = 1 - (\Omega_m + \Omega_{\Lambda})$ ), we run into the degeneracy in Fig. 6. Plotted as colored bands are the  $(\Omega_m, \Omega_{\Lambda})$  confidence contours assuming constant  $h = 0.7$  given  $\delta\mathcal{T}_C = 0.64\%$  from an ensemble with all lenses and sources at  $z_L, z_S = (0.5, 2.0)$ . As  $h$  varies, these contours move as shown.

An ensemble of lenses with a range of redshifts shrinks

the confidence contours somewhat, as we see in Fig. 7, though the strong  $(h, \Omega_m, \Omega_{\Lambda})$  degeneracy remains. Even adopting an aggressive 3% prior on  $h$ , we find neither  $\Omega_m$  nor  $\Omega_{\Lambda}$  can be constrained individually. However, the degeneracy does exhibit a strong preference toward a flat or nearly flat universe. Finally, we note the  $(h, \Omega_m, \Omega_{\Lambda})$  degeneracy can be more cleanly broken if our ensemble includes a significant fraction of lenses at  $z_L = 1$  and higher.

#### 4.3. Flat universe with constant dark energy EOS ( $h, \Omega_{de} = 1 - \Omega_m, w$ )

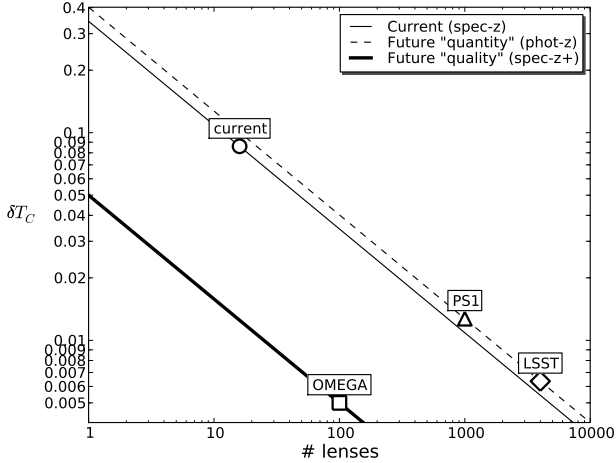


FIG. 3.— Constraints on  $\delta\mathcal{T}_C$  as a function of ensemble size and observational uncertainties. The current ensemble has time delays measured to roughly  $\Delta(\Delta\tau) = 2$  day precision and spectroscopic redshifts measured for all lenses and sources. Future large surveys (“quantity”) should have similar time delay precisions but photometric redshifts measured for lenses ( $\Delta z_L = 0.04(1 + z_L)$ ) and sources ( $\Delta z_S = 0.10(1 + z_S)$ ). A dedicated campaign (“quality”) could in principle obtain tight lens model constraints ( $\delta\Xi_C = 5\%$ ) with high-precision time delays ( $\Delta(\Delta\tau) = 0.1$  day) and spectroscopic redshifts.

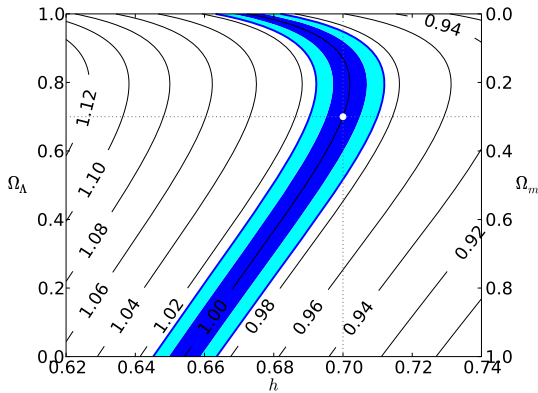


FIG. 4.— Confidence contours (1- and 2- $\sigma$  colored bands) for  $(h, \Omega_\Lambda = 1 - \Omega_m)$  given “Stage IV”  $\delta\mathcal{T}_C = 0.64\%$  obtained from an ensemble with all lenses and sources at  $z_L, z_S = (0.5, 2.0)$ . Here we assume a flat universe with a cosmological constant ( $w = -1$ ). Also plotted are contours of constant  $\Xi_C \equiv \mathcal{T}_C/\mathcal{T}_{C,\text{true}}$ , where  $\mathcal{T}_{C,\text{true}} \approx 0.99$  for the input redshifts and cosmology. The input cosmology  $(h, \Omega_m, \Omega_\Lambda) = (0.7, 0.3, 0.7)$  is marked with dotted lines and a white dot.

Current cosmological constraints are consistent with a flat universe with a cosmological constant (as explored in §4.1). As a first perturbation to this model, it is common to explore constraints on  $w \neq -1$  while maintaining constant  $w$  in a flat universe. This cosmology has three free parameters  $(h, \Omega_{de}, w)$  with  $\Omega_m = 1 - \Omega_{de}$ .

Given enough data and appropriate priors, time delay lenses could place strong constraints on the dark energy equation of state parameter  $w$  (see §5.2). Figs. 8 and 9 explore the dependence of  $\mathcal{T}_C$  on  $(w, \Omega_{de})$  assuming a flat universe and constant  $w$ .

#### 4.4. Flat universe with time-variable dark energy EOS $(h, \Omega_{de} = 1 - \Omega_m, w_0, w_a)$

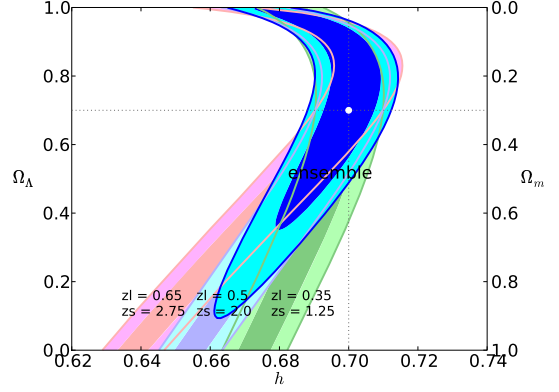


FIG. 5.— Confidence contours (1- and 2- $\sigma$  colored bands) for  $(h, \Omega_\Lambda = 1 - \Omega_m)$  given  $\delta\mathcal{T}_C = 0.64\%$  and assuming a flat universe with a cosmological constant ( $w = -1$ ). Each of the three fainter curves corresponds to all lenses and sources at the same pair of redshifts:  $z_L, z_S = (0.65, 2.75), (0.5, 2.0), (0.35, 1.25)$ , as marked. Next we consider an ensemble of lenses and sources with Gaussian redshift distributions:  $z_L, z_S = (0.5 \pm 0.15, 2.0 \pm 0.75)$ . These yield the tighter constraints (marked “ensemble”). The input cosmology  $(h, \Omega_m, \Omega_\Lambda) = (0.7, 0.3, 0.7)$  is marked with a white dot.

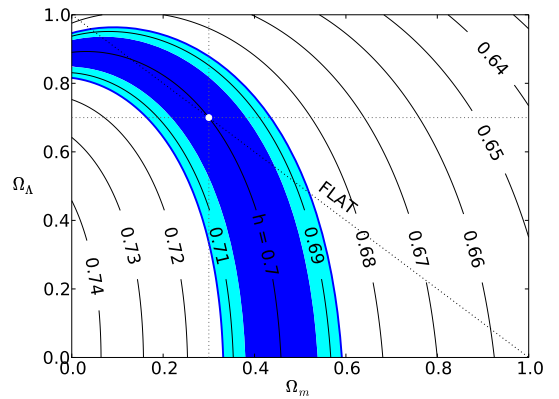


FIG. 6.— Confidence contours (1- and 2- $\sigma$  colored bands) for  $(\Omega_m, \Omega_\Lambda)$  given  $\delta\mathcal{T}_C = 0.64\%$  obtained from an ensemble with all lenses and sources at  $z_L, z_S = (0.5, 2.0)$ . The colored bands shift in  $(\Omega_m, \Omega_\Lambda)$  space as  $h$  varies. A cosmological constant ( $w = -1$ ) is assumed. The input cosmology  $(h, \Omega_m, \Omega_\Lambda) = (0.7, 0.3, 0.7)$  is marked with a white dot. Flat cosmologies lie along the dotted line, and this line’s intersection with the colored bands explains the strange shape of the colored bands in the previous plot.

The most interesting constraints we can hope to place on dark energy are to verify or falsify the following:  $w = -1$  (cosmological constant) and  $w_a = 0$  (constant  $w$ ). In Fig. 10 we explore the dependence of  $\mathcal{T}_C$  on  $(w_0, w_a)$  (see Eq. 10). The colored bands are the constraints we could obtain given perfect knowledge of  $(h, \Omega_m, \Omega_{de})$ . The solid lines on the left show the curves’ migration as a function of  $h$ . On the right, we also explore dependence on  $\Omega_{de}$  for a flat universe ( $\Omega_m + \Omega_{de} = 1$ ).

## 5. COSMOLOGICAL CONSTRAINTS FROM FUTURE EXPERIMENTS

We now consider the full parameter space  $(h, \Omega_m, \Omega_{de}, \Omega_k, w_0, w_a)$  and derive the constraints that may be placed on these parameters given constraints on  $\mathcal{T}_C$  along with various priors. Stage IV time delay constraints are compared to those expected from other experiments as estimated by the Dark Energy

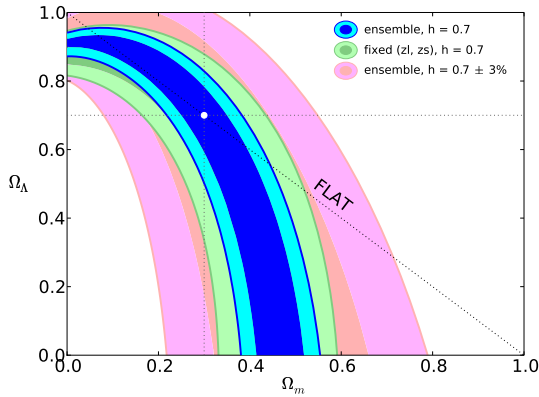


FIG. 7.— Additional confidence contours for  $(\Omega_m, \Omega_\Lambda)$ . The middle set of contours was plotted in the previous figure. The top set of contours assumes an ensemble of lenses and sources  $z_L, z_S = (0.5 \pm 0.15, 2.0 \pm 0.75)$ . Finally, the bottom set of contours is for the ensemble and allowing a 3% uncertainty in  $h$ .

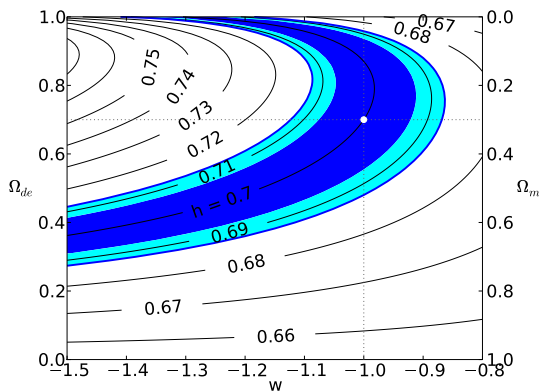


FIG. 8.— Confidence contours (1- and 2- $\sigma$  colored bands) for  $(w, \Omega_{de} = 1 - \Omega_m)$  assuming a flat universe with constant  $w$  given  $\delta\mathcal{T}_C = 0.64\%$  obtained from an ensemble with all lenses and sources at  $z_L, z_S = (0.5, 2.0)$ . The colored bands shift in  $(w, \Omega_{de})$  space as  $h$  varies. The input cosmology  $(h, \Omega_{de}, w) = (0.7, 0.7, -1)$  is marked with a white dot.

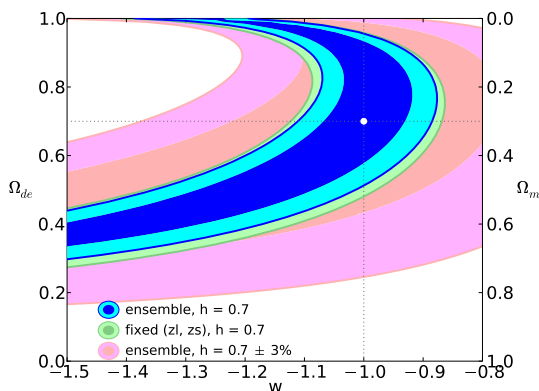


FIG. 9.— Confidence contours for  $(w, \Omega_{de} = 1 - \Omega_m)$ , assuming a flat universe. As in Fig. 7, we plot a “Stage IV” ensemble of lenses at a range of redshifts, the lenses all at the same redshift, and the ensemble allowing 3% uncertainty in  $h$ .

TABLE 3  
STAGE IV FISHER MATRIX EXPECTATION FOR  $(h, \Omega_{de}, \Omega_k, w_0, w_a)$   
GIVEN  $\delta\mathcal{T}_C = 0.64\%$

	$h$	$\Omega_{de}$	$\Omega_k$	$w_0$	$w_a$
$h$	49824.9224	-1829.7018	-4434.2995	4546.8899	122.5319
$\Omega_{de}$	-1829.7018	88.3760	200.9795	-189.2658	-8.4386
$\Omega_k$	-4434.2995	200.9795	463.5732	-445.5690	-17.9694
$w_0$	4546.8899	-189.2658	-445.5690	441.9725	15.2981
$w_a$	122.5319	-8.4386	-17.9694	15.2981	1.0394

Task Force (Albrecht et al. 2006, 2009). To efficiently explore this parameter space, we perform Fisher matrix analyses.

### 5.1. Fisher Matrix Analysis

The Fisher matrix formalism provides a simple way to study uncertainties of many correlated parameters. Constraints from various experiments and/or specific priors may be combined with ease. A “quick-start” instructional guide and software are provided in a companion paper (Coe 2009). Fisher matrices approximate all uncertainties as Gaussians. The true uncertainties may be somewhat higher and non-Gaussian. The full information of the dependencies as shown in §4 is not retained. Yet as cosmological parameters are constrained close to their true values, these approximations should suffice.

As above we consider a “Stage IV” ensemble of time delays which constrains  $\mathcal{T}_C$  to 0.64% with Gaussian distributions of lens and source redshifts ( $z_L = 0.5 \pm 0.15$ ;  $z_S = 2.0 \pm 0.75$ ). Assuming such a Gaussian distribution for  $\mathcal{T}_C$  and the aforementioned redshift ensemble, we calculate (numerically) the Fisher matrix for cosmological parameters of interest. The Fisher matrix consists of partial derivatives of  $\chi^2$  with respect to the parameters. For parameters  $(p_i, p_j)$ , element  $(i, j)$  in the Fisher matrix is given by

$$F_{ij} = \frac{1}{2} \frac{\partial^2 \chi^2}{\partial p_i \partial p_j}. \quad (20)$$

The Stage IV ( $\delta\mathcal{T}_C = 0.64\%$ ) time delay Fisher matrix is given in Table 3 for the cosmological parameters  $(h, \Omega_{de}, \Omega_k, w_0, w_a)$ . The Fisher matrix may be easily scaled to other  $\delta\mathcal{T}_C$  values. For example, to scale from LSST (4,000 lenses;  $\delta\mathcal{T}_C = 0.64\%$ ) to Pan-STARRS 1 (1,000 lenses;  $\delta\mathcal{T}_C = 1.27\%$ ), simply divide all the values in the Fisher matrix by  $4 = 4,000/1,000 = (1.27/0.64)^2$ . Or multiply them by  $1.6 = (0.64/0.4)^2$  to explore the LSST + OMEGA constraints ( $\delta\mathcal{T}_C = 0.4\%$ ). If one is interested in constraints on  $\Omega_m = 1 - (\Omega_{de} + \Omega_k)$ ,  $\omega_m \equiv \Omega_m h^2$ , or any other related variable, a transformation of variables can be performed as outlined in Coe (2009).

In Fig. 11 we show the time delay constraints possible on all parameters and pairs of parameters assuming perfect knowledge of all the other parameters. These plots can be compared to those presented in §4. Such perfect priors are unrealistic, but they help to demonstrate the parameter dependencies and degeneracies.

### 5.2. Flat universe with constant $w$

We first consider the simple case of a flat universe with constant  $w$ . This is a common perturbation to the con-

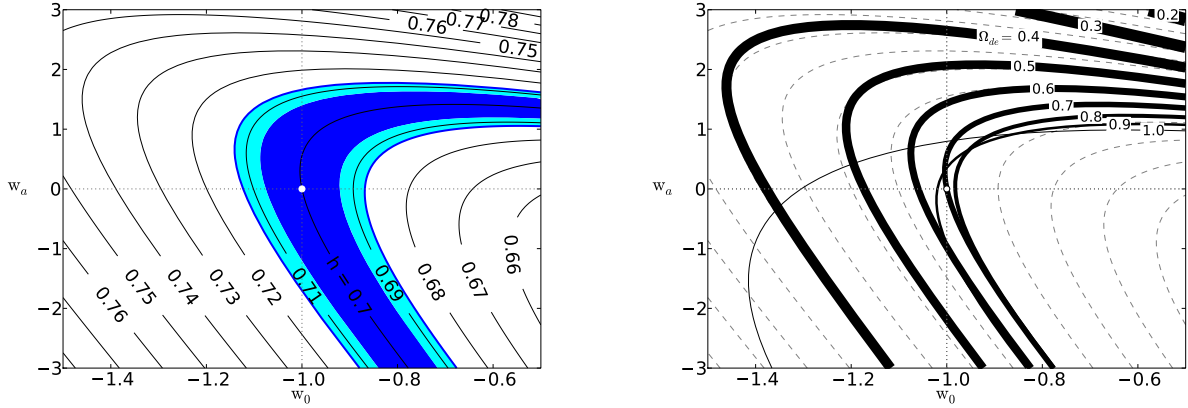


FIG. 10.— *Left:* Confidence contours (1- and 2- $\sigma$  colored bands) for  $(w_0, w_a)$  given  $\delta\mathcal{T}_C = 0.64\%$  obtained from an ensemble with all lenses and sources at  $z_L, z_S = (0.5, 2.0)$  and assuming  $h = 0.7$  and perfect knowledge of  $(\Omega_m, \Omega_{de})$ . As shown, these bands shift in  $(w_0, w_a)$  space as  $h$  varies. The input cosmology  $(h, w_0, w_a) = (0.7, -1, 0)$  is marked with a white dot. *Right:* Dependence of the  $(w_0, w_a)$  contours on  $\Omega_{de}$ , assuming a flat cosmology. Dashed lines show the  $h$  dependence from the left plot. Solid lines of increasing thickness show contours of  $\Omega_{de}$  decreasing in 0.1 increments.

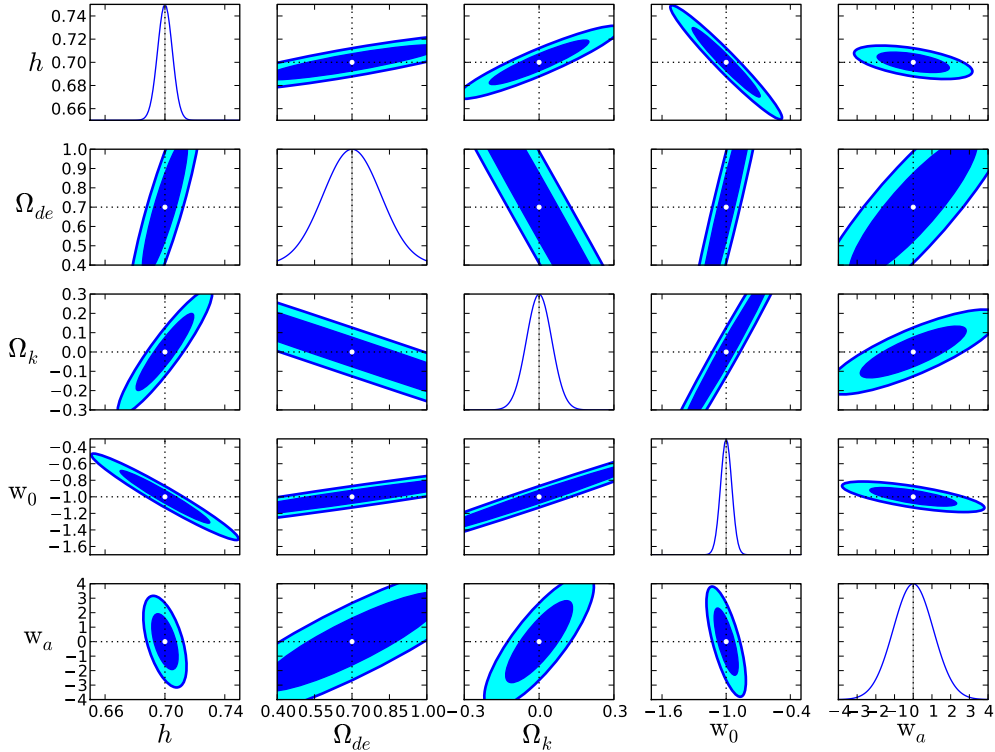


FIG. 11.— Constraints placed on pairs of parameters derived from our Fisher matrix analysis assuming perfect knowledge of all other parameters given  $\delta\mathcal{T}_C = 0.64\%$  obtained from an ensemble with Gaussian distributions of lens and source redshifts ( $z_L = 0.5 \pm 0.15$ ;  $z_S = 2.0 \pm 0.75$ ). All off-diagonal plots show 1- and 2- $\sigma$  colored ellipses. Along the diagonal are constraints on individual parameters assuming perfect knowledge of all others. The y axes along the diagonal are units of relative probability, different from the off-diagonal plots.

cordance cosmology. The goal is to detect deviation from  $w = -1$ , equivalent to the cosmological constant  $\Lambda$ . This 3-parameter cosmology ( $h, \Omega_{de}, w$ , with  $\Omega_m = 1 - \Omega_{de}$ ) was explored above in §4.3.

The top row of Fig. 12 shows Stage IV time delay constraints with a Planck prior in a flat universe with constant  $w$ . Given these priors, we estimate that time delays will constrain  $h$  to 0.007 ( $\sim 1\%$ ),  $\Omega_{de}$  to 0.005, and  $w$  to 0.026 (all 1- $\sigma$  precisions).

In the bottom row of Fig. 12, we compare these time delay constraints (TD) to those expected from other methods: weak lensing (WL), baryon acoustic oscillations (BAO), supernovae (SN), and cluster counts (CL). We consider “optimistic Stage IV” expectations from these methods as calculated by the Dark Energy Task Force (DETF; Albrecht et al. 2006, 2009) and made available in the software DETFast<sup>9</sup>. A Planck prior (also calculated by the DETF) is again assumed for all experiments.

In manipulating the DETF Fisher matrices we adopt their cosmology  $(\Omega_m, \Omega_{de}, h) = (0.27, 0.73, 0.72)$ , but we revert to our chosen cosmology  $(\Omega_m, \Omega_{de}, h) = (0.3, 0.7, 0.7)$  for the rest of our analysis. These differences have negligible impact on our results.

Lewis & Ibata (2002) considered similar constraints from time delay lenses but found much weaker constraints on  $(h, w)$ , even with all other cosmological parameters fixed. One of the cases they considered was 500 lenses with 15% uncertainty each, which translates to  $15\%/\sqrt{500} = 0.66\%$  total uncertainty, very similar to the 0.64% uncertainty we estimate for LSST given 4,000 lenses with a much higher uncertainty (effectively 40%) assumed per lens. For this case, they find  $0.99 \lesssim h \lesssim 1.10$  and  $-1.48 \lesssim w \lesssim -0.88$  (95% confidence). When we perform a similar analysis, assuming  $\delta\mathcal{T}_C = 0.64\%$  and perfect knowledge of  $(\Omega_m, \Omega_{de}, \Omega_k, w_a)$ , we obtain similar uncertainties (without biases, by construction):  $h = 0.7 \pm 0.02$  and  $w = -1 \pm 0.21$  (1- $\sigma$ ). But with the addition of a Planck prior, even while relaxing the perfect prior on  $(\Omega_m, \Omega_{de}, \Omega_k, w_a)$ , we find improved constraints of  $h = 0.7 \pm 0.007$  and  $w = -1 \pm 0.026$  (1- $\sigma$ ). Planck clearly complements the strong lensing constraints well to produce tight constraints on  $(h, w)$ .

### 5.3. General Cosmology

We now assume a general cosmology allowing for curvature and a time-varying  $w$ . To help constrain this larger parameter space ( $h, \Omega_{de}, \Omega_k, w_0, w_a$ , with  $\Omega_m = 1 - (\Omega_{de} + \Omega_k)$ ), we add additional priors. In addition to the Planck prior, we adopt “Stage II” (near-future) constraints from weak lensing (WL) + supernovae (SN) + cluster counts (CL), all as calculated by the DETF. The DETF uses this prior (in addition to Planck) in many of their calculations comparing the performance of Stage III – IV techniques.

The Stage II DETF WL + SN + CL prior yields the following uncertainties:  $\Delta h = 0.031$  (4.4%),  $\Delta\Omega_{de} = 0.023$ ,  $\Delta\Omega_k = 0.010$ ,  $\Delta w_0 = 0.128$ ,  $\Delta w_a = 0.767$  (along with various covariances between parameters). The addition of the Planck prior reduces these to:  $\Delta h = 0.017$  (2.4%),  $\Delta\Omega_{de} = 0.012$ ,  $\Delta\Omega_k = 0.003$ ,  $\Delta w_0 = 0.115$ ,

$\Delta w_a = 0.525$ . Note that Stage II WL+SN+CL constrains  $h$  well enough (to 4.4%) that an HST Key Project prior ( $h = 0.72 \pm 0.08$ ) appears to be unnecessary. Even SHOES ( $h = 0.742 \pm 0.036$ , or 4.9%) provides a weaker constraint on  $h$ . However, as noted in the introduction, these combined WL+SN+CL experiments yield a prediction of  $h$  based on an assumed cosmological model and are no substitute for local measurements of  $h$  (Riess et al. 2009).

These Stage II constraints are also rather optimistically combined, assuming that all experiments have converged on the same best fit cosmology without systematic offsets among them. The true Stage II constraints should be somewhat weaker.

Plotted in Fig. 13 are time delay constraints assuming a prior of Planck + Stage II WL+SN+CL. A progression is shown from Stage I (present) time delay constraints ( $\delta\mathcal{T}_C = 8.6\%$ ) through Stage II ( $\delta\mathcal{T}_C = 1.27\%$ ) and on to Stage IV ( $\delta\mathcal{T}_C = 0.64\%$ ). The current constraints barely improve upon this aggressive prior. While the Stage II – IV constraints certainly improve upon the prior, note that the outer bounds of the time delay and prior ellipses nearly intersect. This indicates that the size of the time delay ellipse is controlled by that of the prior, at least for these constraints and prior. Were the prior significantly weaker or the time delay constraints significantly stronger, we have verified that the time delay ellipses would shrink well within the prior ellipses.

In Fig. 14 we compare Stage IV time delay constraints to those expected from other methods for various parameters of interest. Plotted are constraints on  $(h, \Omega_k)$ ,  $(h, w_0)$ , and  $(w_0, \Omega_k)$ , and  $(w_0, w_a)$ . An example of how these constraints combine is given in §5.4.2.

We give extra attention to constraints on the dark energy parameters  $(w_0, w_a)$ . The DETF figure of merit (FOM) for a given experiment is defined as the inverse of the area of the ellipse in the  $(w_0, w_a)$  plane. In Fig. 15 we plot FOM for various experiments versus the “pivot redshift”, defined as follows. For a time-varying  $w(z)$ , time delays constrain  $w$  best at  $z \approx 0.31$ . This redshift is known as the pivot redshift (Huterer & Turner 2001; Hu & Jain 2004) and can also be calculated simply from the  $(w_0, w_a)$  constraints (Coe 2009). As in the previous plot, we assume a prior of Planck + Stage II (WL+SN+CL).

### 5.4. Time delays do not simply constrain $h$

#### 5.4.1. Relaxing the “perfect prior” on $(\Omega_m, \Omega_{de}, \Omega_k, w_0, w_a)$

To date, analyses of time delay lenses have quoted uncertainties on  $\mathcal{T}_C$  as uncertainties on  $h$ , assuming  $\delta h = \delta\mathcal{T}_C$ . This assumption has been valid to date, but future constraints on  $h$  will be weaker than the constraints on  $\mathcal{T}_C$ , that is  $\delta h > \delta\mathcal{T}_C$ .

This is demonstrated in Fig. 16 *left*. The dashed line shows  $\delta h = \delta\mathcal{T}_C$ , or the “perfect prior” on  $(\Omega_m, \Omega_{de}, \Omega_k, w_0, w_a)$  generally assumed in analyses. For future samples (at the left side of the plot), as this prior is loosened, we find  $\delta h > \delta\mathcal{T}_C$ . In Fig. 16 *right*, we plot  $\delta h/\delta\mathcal{T}_C$ . For example, given a “Stage II” prior on WL+SN+CL, and LSST constraints on time delays ( $\delta\mathcal{T}_C = 0.64\%$ ), we find  $\delta h \sim 2.2\delta\mathcal{T}_C \sim 1.4\%$ . Alternatively, assuming a Planck prior in a flat universe with constant  $w$ , we would find  $\delta h \sim 1.4\delta\mathcal{T}_C \sim 0.90\%$ .

<sup>9</sup> <http://www.physics.ucdavis.edu/DETFast/>

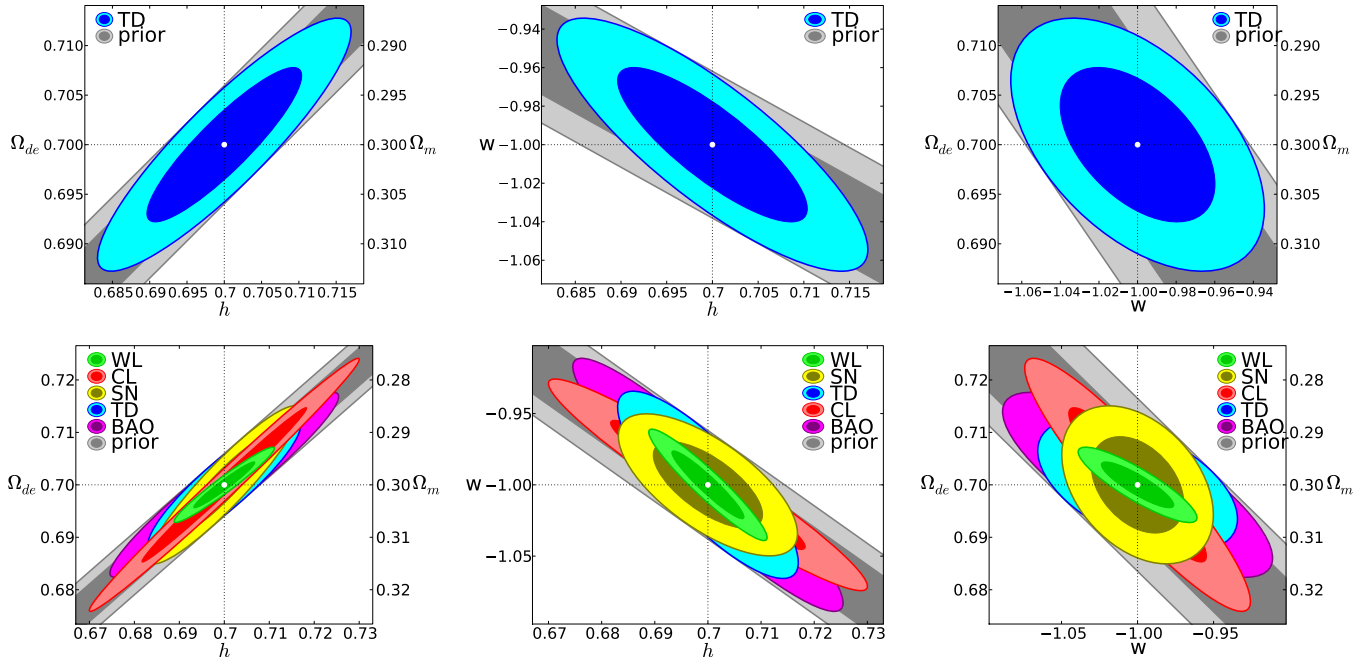


FIG. 12.— *Top row:* Cosmological constraints from “Stage IV” time delays plus a Planck prior in a flat universe with constant  $w$ . We assume an ensemble of time delays which constrains  $\mathcal{T}_C$  to 0.64% (see text for details). Time delays plus Planck constrain  $h$  to 0.007 (1%),  $\Omega_{de}$  to 0.005, and  $w$  to 0.026 (all 1- $\sigma$  precisions). *Bottom row:* Comparison of “optimistic Stage IV” constraints expected from time delays (TD), weak lensing (WL), supernovae (SN), baryon acoustic oscillations (BAO), and cluster counts (CL). The time delay constraints are as plotted in the top row. For the other experiments we use Fisher matrix calculations provided by the Dark Energy Task Force (DETF). For each parameter pair, experiments are plotted in order of FOM  $\propto$  (Ellipse Area) $^{-1}$ , with the best experiment on top.

(Note that the Stage II WL+SN+CL prior claims a constraint of  $\delta h = 0.03$ , such that it outperforms current constraints from time delays  $\delta h = \delta \mathcal{T}_C$ .)

#### 5.4.2. Time delays provide more than constraints on $h$

In the introduction we commented on the ability of any experiment to improve constraints on  $w$  and  $\Omega_k$  simply by tightening the constraints on  $h$ . Several methods have the potential to further improve the constraints on  $h$  (Olling 2007). Do time delays offer more than a simple constraint on  $h$  for the purposes of constraining the dark energy equation of state?

In Fig. 17 we compare Stage IV time delays (*left*) to a simple  $h$  constraint (*right*) in ability to constrain dark energy. Each is combined with Stage IV supernovae constraints plus a prior of Planck + Stage II WL+SN+CL.<sup>10</sup> We find time delays are more powerful than the simple  $h$  constraint. The (SN + TD + prior) figure of merit (FOM) on  $(w_0, w_a)$  is  $\sim 19\%$  higher than that from (SN + H + prior).

The “H” constraint  $\delta h = 0.009$  was chosen such that when combined with the prior, the resulting  $\delta h$  would equal that from TD + prior. Both H + prior and TD + prior yield  $\delta h = 0.008$ . However we find TD outperforms even a perfect H prior ( $\delta h \sim 0$ ) by 13%. Simply put, the time delay constraints on  $(\Omega_m, \Omega_{de}, \Omega_k, w_0, w_a)$  are clearly making contributions.

When combined with experiments other than SN, TD offers less marked improvements over H constraints. Re-

placing SN with BAO, WL, and CL, we find TD outperforms H by 7%, 5%, and 3%, respectively.

#### 5.5. Lens and Source Redshift Distribution

We have been considering the Gaussian redshift distributions  $z_L = 0.5 \pm 0.15$ ,  $z_S = 2.0 \pm 0.75$  introduced by Dobke et al. (2009) as reasonable approximate assumptions for near-future missions. We find that the cosmological parameter constraints are not extremely sensitive to variations in these redshift distributions.

For  $\delta \mathcal{T}_C = 0.64\%$  plus our Planck + Stage II (WL+SN+CL) prior, we find the following. A lower tighter lens redshift distribution of  $z_L = 0.2 \pm 0.1$  improves the constraint on  $h$  by 22% and on  $\Omega_{de}$  by 12% at the expense of the  $w_0$  and  $w_a$  constraints, which degrade by 8% and 10%, respectively. A higher tighter lens redshift distribution of  $z_L = 1.0 \pm 0.1$  has less leverage, as the  $h$  and  $\Omega_{de}$  constraints degrade by 15% and 14%, respectively with little benefit to the other parameters. Neither broader lens redshift distributions nor variations on the source redshift distribution have much impact on the parameter constraints.

When time delay constraints are tighter ( $\delta \mathcal{T}_C < 0.64\%$ ), with the same priors, the lens redshift distribution begins to have a greater impact. We reserve study of such “beyond Stage IV” constraints for future work.

## 6. SYSTEMATICS

As with any measurement, there are many potential sources of systematic bias, as alluded to throughout this work. At the risk of putting the cart before the horse, we have presented systematic-free projections for time delay cosmological constraints. These should serve to motivate a more considered look at systematics, in the context of

<sup>10</sup> Strictly speaking we have not taken the proper care in combining constraints from the Stage II and Stage IV supernova experiments, as their nuisance parameters have been marginalized over in the DETF Fisher matrices. But this analysis will suffice for illustrative purposes here.

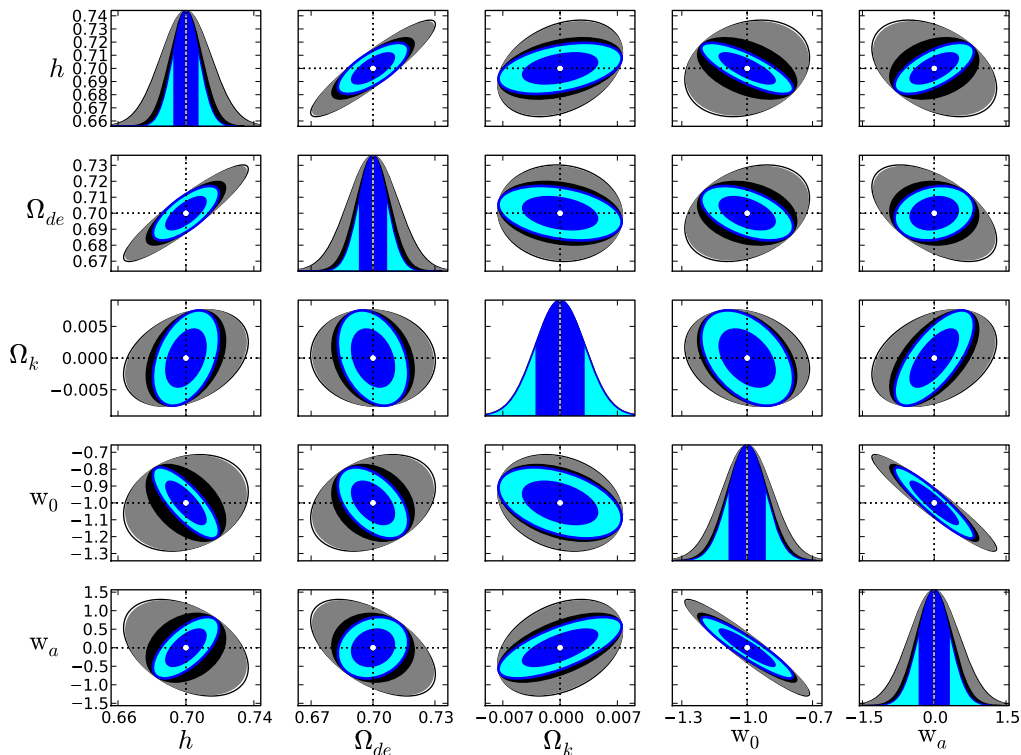


FIG. 13.— Cosmological constraints from time delays in a general cosmology assuming priors of Planck + Stage II (WL+SN+CL) as calculated by the DETF. A progression is shown from the prior (outermost ellipse,  $2\text{-}\sigma$ ) to Stage I (current) time delay constraints ( $\delta\mathcal{T}_C = 8.6\%$ ; gray ellipse,  $2\text{-}\sigma$ ) to Stage II constraints ( $\delta\mathcal{T}_C = 1.4\%$ ; black ellipse,  $2\text{-}\sigma$ ) to Stage IV constraints ( $\delta\mathcal{T}_C = 0.64\%$ ; colored ellipses,  $1\text{-}\sigma$  and  $2\text{-}\sigma$ ). Along the diagonal are plotted constraints on individual parameters marginalizing over all others. The y axes along the diagonal are units of relative probability, different from the off-diagonal plots. For each plot, we marginalize over all other parameters, unlike Fig. 11 in which unrealistic perfect priors were assumed for illustrative purposes.

the behavior of random uncertainties in these studies. Ideally, efforts should be undertaken to reduce systematics on a timescale comparable to that presented here (e.g.,  $0.64\%$  by “Stage IV”). If this cannot be accomplished, we study prospects for estimating cosmological parameters in spite of large residual systematic biases in Paper III (Coe & Moustakas 2009c).

Here we discuss briefly the greatest potential sources of systematic bias. We should consider which of our main sources of statistical uncertainty (lens modelling, redshift measurements, and time delay measurements) could also contribute significant systematic bias. Time delay uncertainties are generally not expected to be biased in any preferred direction. Redshift biases are somewhat worrisome but will not be discussed further here. Most daunting are potential biases due to imprecise lens modeling.

Whether we determine the appropriate lens model for the “typical” (“average”) lens in an ensemble or we constrain each individual lens model well, we must use the following tools to measure lens properties. The largest statistical uncertainties and potential systematic biases involve measurements of the lens mass density slope and perturbing mass sheets.

### 6.1. Lens Mass Density Slope

Regarding mass slope, this paper has focused on the statistical strategy which assumes that we know the correct mean of mass slopes. Evidence currently suggests that lenses are isothermal ( $\alpha = 1$ ,  $\gamma = 2$ )<sup>11</sup> on average. Yet a recent analysis of 58 SLACS lenses finds a slightly higher average slope of  $\gamma = 2.085^{+0.025}_{-0.018}(\text{stat.}) \pm 0.1(\text{syst.})$  (Koopmans et al. 2009b). If the average proved to be exactly  $\gamma = 2.085$ , this would result in an  $8.5\%$  bias in  $\mathcal{T}_C$  ( $\delta\mathcal{T}_C = \delta\gamma/2 = \delta\alpha$ ) were we to assume an average of  $\gamma = 2$  instead.

Mass profile slopes for individual lenses are determined by measuring mass within two radii: the Einstein radius (from the positions of multiple images) and a smaller radius (from velocity dispersions). The latter require detailed spectroscopy (e.g., Koopmans et al. 2006). It will not be feasible to obtain the required measurements for all time delay lenses detected in future surveys, but small samples of these can be selected for such detailed study.

### 6.2. Mass Sheets

Mass sheets can be equally harmful as a source of systematics as  $\mathcal{T}_C$  bias also scales linearly with projected

<sup>11</sup> We use two definitions common in the literature regarding lens slope: two-dimensional mass surface density  $\kappa \propto r^{2-\alpha}$ , and three-dimensional mass surface density  $\rho \propto r^{-\gamma}$ . These parameters are related by  $\alpha + \gamma \approx 3$  (see discussion in van de Ven et al. 2009).

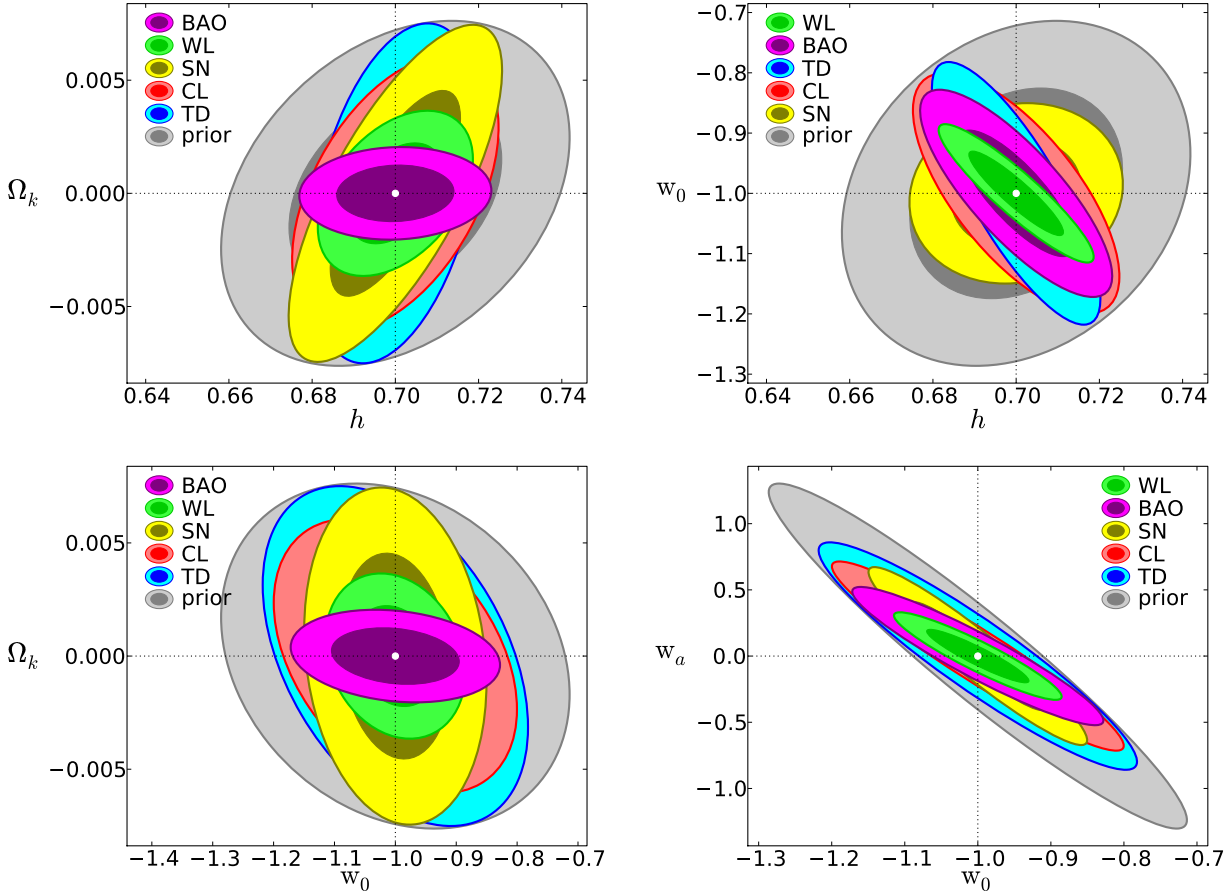


FIG. 14.— Comparisons of “Stage IV” constraints possible from time delays (TD), weak lensing (WL), supernovae (SN), baryon acoustic oscillations (BAO), and cluster counts (CL) in a general cosmology (allowing for curvature and a time-variable  $w$ ). For TD, we assume an ensemble which constrains  $\mathcal{T}_C$  to 0.64% (see text for details). For the rest we use “optimistic Stage IV” expectations calculated from Fisher matrices provided by the Dark Energy Task Force (DETF). A prior of Planck + Stage II (WL+SN+CL) is assumed for all five experiments and is plotted in gray. For each parameter pair, experiments are plotted in order of FOM  $\propto$  (Ellipse Area) $^{-1}$ , with the best experiment on top.

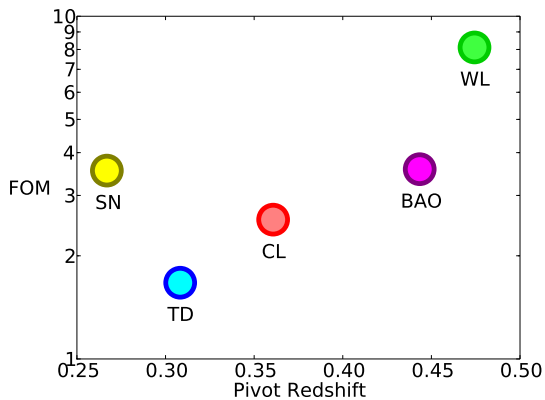


FIG. 15.— Dark energy figure of merit (FOM  $\propto$   $((w_0, w_a)$  Ellipse Area) $^{-1}$ , normalized relative to the prior) versus pivot redshift for various “optimistic Stage IV” experiments with a prior of Planck + Stage II (WL+SN+CL). The pivot redshift is the redshift at which  $w(z)$  is best constrained.

mass density,  $\delta\mathcal{T}_C \sim \kappa$ . Mass sheets can result from both mass within the lens group environment and mass along the line of sight (over- or under-densities) all the way from source to observer. The former is the dominant effect. Simulations (Dalal & Watson 2005) suggest

that group members contribute  $\kappa_{\text{env}} = 0.03 \pm 0.6$  dex (i.e.,  $\log_{10}(\kappa_{\text{env}}) = \log_{10}(0.03) \pm 0.6$ ) for a 1- $\sigma$  upper bound of  $\kappa_{\text{env}} = 0.12$ , or 12% bias on  $\mathcal{T}_C$ . Mass along the line of sight is generally lower and more nearly fluctuates about the cosmic average but should also be accounted for. Hilbert et al. (2007) measured mass along the lines of sight to strong lenses in the Millennium simulation. For sources at  $z_S = 2$ , the central 68% span  $-0.0355 < \kappa_{\text{los}} < 0.0475$  (Paper I).

Efforts are made to measure  $\kappa_{\text{env}}$  for individual lenses via spectroscopic (and photometric) studies (e.g., Momcheva et al. 2006; Auger 2008) and simulations which estimate the effects of nearby neighbors (e.g., Keeton & Zabludoff 2004; Dalal & Watson 2005). Similar studies also attempt to identify groups along the line of sight and estimate their mass sheet contributions (e.g., Fassnacht et al. 2006).

The alternative is a statistical approach. Measurements of  $\kappa_{\text{env}}$  or  $\kappa_{\text{los}}$  would not be required for individual lenses if we had knowledge of the distributions  $P(\kappa_{\text{env}})$  and  $P(\kappa_{\text{los}})$  for strong lenses. These distributions could be obtained from simulations, and one could attempt to correct for the expected bias for lenses to reside in high density regions (Dalal & Watson 2005; Oguri et al. 2005). However, one might wonder whether these dis-

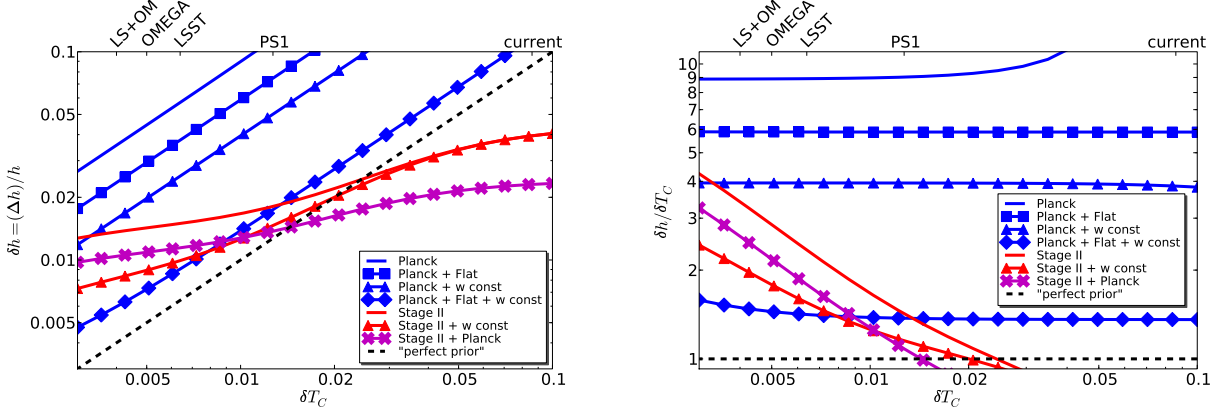


FIG. 16.— Demonstration that  $\delta h > \delta \mathcal{T}_C$  for future ensembles. *Left*: Constraints on  $h$  versus constraints on  $\mathcal{T}_C$  for various priors. Along the top horizontal axis we plot experiments with corresponding  $\delta \mathcal{T}_C$ : current constraints (8.6%), Pan-STARRS 1 (1.27%), LSST (0.64%), OMEGA (0.5%), and LSST + OMEGA (0.4%). The priors are different combinations of the following: Planck, a flat universe, constant  $w$ , and a “Stage II” prior from (WL+SN+CL). This Stage II prior constrains  $\Omega_k$  to 0.01, so the additional prior of flatness helps it little here. The bottom line is the “perfect prior”, perfect knowledge of  $(\Omega_{de}, \Omega_m, \Omega_k, w_0, w_a)$  as is generally assumed, for which  $\delta \mathcal{T}_C = \delta h$ . *Right*: Relative constraints on  $h$  compared to the perfect prior. For example, given the Stage II prior, we find  $\delta h \sim 2.2\delta \mathcal{T}_C$ .

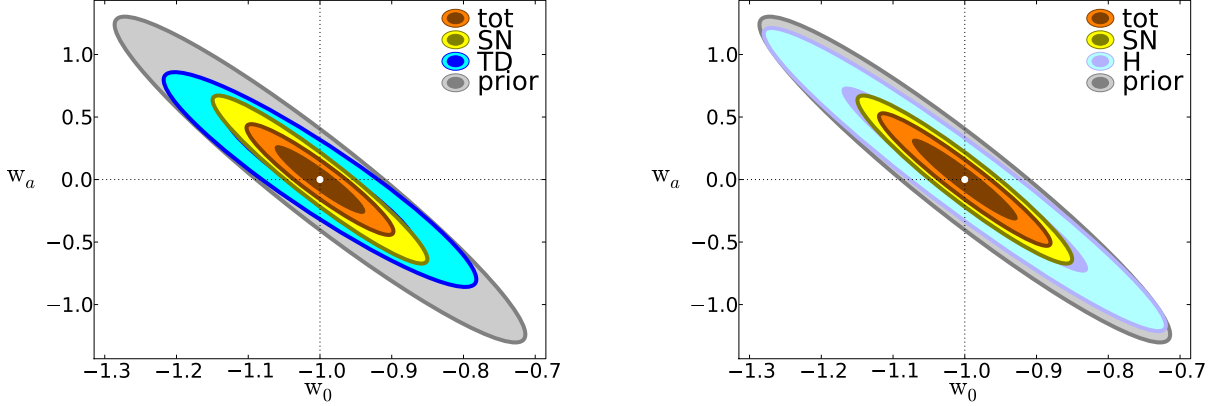


FIG. 17.— *Left*: Combined constraints on  $(w_0, w_a)$  from Stage IV time delays (TD) and supernovae (SN). A prior of Planck + Stage II (WL+SN+CL) is assumed. The TD + prior constraint yields  $\delta h = 0.008$  (not shown). *Right*: Similar plot combining Stage IV SN with a  $\delta h = 0.009$  constraint on Hubble’s constant (that which also yields  $\delta h = 0.008$  when combined with the prior). Time delays yield a 19% improvement in figure of merit ( $\text{FOM} \propto ((w_0, w_a) \text{ Ellipse Area})^{-1}$ ), versus the constraint on  $h$  alone. SN + TD shows the most dramatic improvement vs. SN + H. Replacing SN with the other experiments (BAO, WL, CL) we find lesser improvements vs. H of 7%, 5%, and 3%, respectively.

tributions and corrections would prove accurate to the percent level. Any errors would yield residual systematics in our estimation of  $\mathcal{T}_C$ .

To aid such a statistical approach, lenses in obvious groups can be excluded from the analysis leaving only those systems with low  $\kappa_{\text{env}}$ . Such low mass systems would introduce smaller biases, though a detailed exploration of this approach will await future work.

## 7. CONCLUSIONS

We have presented the first analysis of the potential of gravitational lens time delays to constrain a broad range of cosmological parameters. The cosmological constraining power  $\delta \mathcal{T}_C$  was calculated for Pan-STARRS 1, LSST, and OMEGA based on expected numbers of lenses (including the quad-to-double ratio) as well as the expected uncertainties in lens models, photometric redshifts, and time delays. Our Fisher matrix results are provided to allow time delay constraints to be easily combined with and compared to constraints from other methods.

We concentrate on “Stage IV” constraints from LSST.

In a flat universe with constant  $w$  including a Planck prior, LSST time delay measurements for  $\sim 4,000$  lenses should constrain  $h$  to  $\sim 0.007$  ( $\sim 1\%$ ),  $\Omega_{de}$  to  $\sim 0.005$ , and  $w$  to  $\sim 0.026$  (all  $1\text{-}\sigma$  precisions). We compare these results as well as those for a general cosmology to other “optimistic Stage IV” constraints expected from weak lensing, supernovae, baryon acoustic oscillations, and cluster counts, as calculated by the Dark Energy Task Force (DETF).

Combined with appropriate priors (those adopted by the DETF), time delays provide modest constraints on a time-varying  $w(z)$  that complement the constraints expected from other methods. Time delays constrain  $w$  best at  $z \approx 0.31$ , the “pivot redshift” for this method.

We find that LSST and OMEGA represent about an even trade in “quantity versus quality” in terms of constraining cosmology with time delays. LSST could yield  $\delta \mathcal{T}_C \sim 0.64\%$  by measuring time delays for 4,000 lenses, while OMEGA could yield  $\delta \mathcal{T}_C \sim 0.5\%$  by obtaining high-precision time delay measurements and lens model

constraints for 100 lenses with spectroscopic redshifts. The combined statistical power of these two missions could further improve the cosmological constraints to  $\delta\mathcal{T}_C \sim 0.4\%$ .

We acknowledge useful conversations with Phil Marshall, Matt Auger, Chuck Keeton, Chris Kochanek, Ben Dobke, Chris Fassnacht, Lloyd Knox, Jason Dick, An-

dreas Albrecht, Tony Tyson, and Jason Rhodes. We are grateful to the DETF for releasing Fisher matrices detailing their estimates of cosmological constraints from various experiments. We thank the referee for useful comments which led us to significantly improve the manuscript. This work was carried out at Jet Propulsion Laboratory, California Institute of Technology, under a contract with NASA.

## REFERENCES

- Albrecht, A., Amendola, L., Bernstein, G., Clowe, D., Eisenstein, D., Guzzo, L., Hirata, C., Huterer, D., et al. 2009, ArXiv e-prints [ADS]
- Albrecht, A., Bernstein, G., Cahn, R., Freedman, W. L., Hewitt, J., Hu, W., Huth, J., Kamionkowski, M., et al. 2006, ArXiv Astrophysics e-prints [ADS]
- Auger, M. W. 2008, MNRAS, 383, L40 [ADS]
- Blake, C. A., Abdalla, F. B., Bridle, S. L., & Rawlings, S. 2004, New Astronomy Review, 48, 1063 [ADS]
- Blandford, R. & Narayan, R. 1986, ApJ, 310, 568 [ADS]
- Bolton, A. S., Burles, S., Koopmans, L. V. E., Treu, T., & Moustakas, L. A. 2006, ApJ, 638, 703 [ADS]
- Braatz, J. 2009, Astronomy, 2010, 23 [ADS]
- Braatz, J. A., Reid, M. J., Greenhill, L. J., Condon, J. J., Lo, K. Y., Henkel, C., Gugliucci, N. E., & Hao, L. 2008, in Astronomical Society of the Pacific Conference Series, Vol. 395, Frontiers of Astrophysics: A Celebration of NRAO's 50th Anniversary, ed. A. H. Bridle, J. J. Condon, & G. C. Hunt, 103–+ [ADS]
- Cabanac, R. A., Alard, C., Dantel-Fort, M., Fort, B., Gavazzi, R., Gomez, P., Kneib, J. P., Le Fèvre, O., et al. 2007, A&A, 461, 813 [ADS]
- Chae, K.-H. 2007, ApJ, 658, L71 [ADS]
- Chevallier, M. & Polarski, D. 2001, International Journal of Modern Physics D, 10, 213 [ADS]
- Coe, D. 2009, ArXiv e-prints [ADS]
- Coe, D., Benítez, N., Sánchez, S. F., Jee, M., Bouwens, R., & Ford, H. 2006, AJ, 132, 926 [ADS]
- Coe, D. A. & Moustakas, L. A. 2009a, in prep. (Paper I)
- , 2009c, in prep. (Paper III)
- Coles, J. 2008, ApJ, 679, 17 [ADS]
- Dalal, N. & Watson, C. R. 2005, in 25 Years After the Discovery: Some Current Topics on Lensed QSOs, ed. L. J. Goicoechea [ADS]
- Dobke, B. M., King, L. J., Fassnacht, C. D., & Auger, M. W. 2009, MNRAS, 397, 311 [ADS]
- Eigenbrod, A., Courbin, F., Vuissoz, C., Meylan, G., Saha, P., & Dye, S. 2005, A&A, 436, 25 [ADS]
- Fassnacht, C. D., Gal, R. R., Lubin, L. M., McKean, J. P., Squires, G. K., & Readhead, A. C. S. 2006, ApJ, 642, 30 [ADS]
- Fassnacht, C. D., Marshall, P. J., Baltz, A. E., Blandford, R. D., Schechter, P. L., & Tyson, J. A. 2004, in Bulletin of the American Astronomical Society, Vol. 36, Bulletin of the American Astronomical Society, 1531–+ [ADS]
- Faure, C., Kneib, J.-P., Covone, G., Tasca, L., Leauthaud, A., Capak, P., Jahnke, K., Smolcic, V., et al. 2008, ApJS, 176, 19 [ADS]
- Freedman, W. L., Madore, B. F., Gibson, B. K., Ferrarese, L., Kelson, D. D., Sakai, S., Mould, J. R., Kennicutt, Jr., R. C., et al. 2001, ApJ, 553, 47 [ADS]
- Fukugita, M., Futamase, T., Kasai, M., & Turner, E. L. 1992, ApJ, 393, 3 [ADS]
- Futamase, T. & Hamaya, T. 1999, Progress of Theoretical Physics, 102, 1037 [ADS]
- Hilbert, S., White, S. D. M., Hartlap, J., & Schneider, P. 2007, MNRAS, 382, 121 [ADS]
- Hogg, D. W. 1999, ArXiv Astrophysics e-prints [ADS]
- Hu, W. 2005, in Astronomical Society of the Pacific Conference Series, Vol. 339, Observing Dark Energy, ed. S. C. Wolff & T. R. Lauer, 215–+ [ADS]
- Hu, W. & Jain, B. 2004, Phys. Rev. D, 70, 043009 [ADS]
- Huterer, D. & Turner, M. S. 2001, Phys. Rev. D, 64, 123527 [ADS]
- Ilbert, O., Arnouts, S., McCracken, H. J., Bolzonella, M., Bertin, E., Le Fèvre, O., Mellier, Y., Zamorani, G., et al. 2006, A&A, 457, 841 [ADS]
- Inada, N., Oguri, M., Becker, R. H., Shin, M.-S., Richards, G. T., Hennawi, J. F., White, R. L., Pindor, B., et al. 2008, AJ, 135, 496 [ADS]
- Ivezic, Z., Tyson, J. A., Allsman, R., Andrew, J., Angel, R., & for the LSST Collaboration. 2008, ArXiv e-prints [ADS]
- Jackson, N. 2007, Living Reviews in Relativity, 10, 4 [ADS]
- Kaiser, N. 2004, in Presented at the Society of Photo-Optical Instrumentation Engineers (SPIE) Conference, Vol. 5489, Society of Photo-Optical Instrumentation Engineers (SPIE) Conference Series, ed. J. M. Oschmann, Jr., 11–22 [ADS]
- Keeton, C. R. 2009, ArXiv e-prints [ADS]
- Keeton, C. R. & Moustakas, L. A. 2009, ApJ, 699, 1720 [ADS]
- Keeton, C. R. & Zabludoff, A. I. 2004, ApJ, 612, 660 [ADS]
- Koopmans, L. V. E., Auger, M., Barnabe, M., Bolton, A., Bradac, M., Ciotti, L., Congdon, A., Czoske, O., et al. 2009a, ArXiv e-prints [ADS]
- Koopmans, L. V. E., Bolton, A., Treu, T., Czoske, O., Auger, M. W., Barnabè, M., Vegetti, S., Gavazzi, R., et al. 2009b, ApJ, 703, L51 [ADS]
- Koopmans, L. V. E., Browne, I. W. A., & Jackson, N. J. 2004, New Astronomy Review, 48, 1085 [ADS]
- Koopmans, L. V. E., Treu, T., Bolton, A. S., Burles, S., & Moustakas, L. A. 2006, ApJ, 649, 599 [ADS]
- Lazio, J. 2008, in American Institute of Physics Conference Series, Vol. 1035, The Evolution of Galaxies Through the Neutral Hydrogen Window, ed. R. Minchin & E. Momjian, 303–309 [ADS]
- Lee, S. & Ng, K.-W. 2007, Phys. Rev. D, 76, 043518 [ADS]
- Lewis, G. F. & Iбата, R. A. 2002, MNRAS, 337, 26 [ADS]
- Linder, E. V. 2003, Physical Review Letters, 90, 091301 [ADS]
- , 2004, Phys. Rev. D, 70, 043534 [ADS]
- Marshall, P., Blandford, R., & Sako, M. 2005, New Astronomy Review, 49, 387 [ADS]
- Marshall, P. J., Auger, M., Bartlett, J. G., Bradac, M., Cooray, A., Dalal, N., Dobler, G., Fassnacht, C. D., et al. 2009a, ArXiv e-prints [ADS]
- Marshall, P. J., Hogg, D. W., Moustakas, L. A., Fassnacht, C. D., Bradač, M., Schrabback, T., & Blandford, R. D. 2009b, ApJ, 694, 924 [ADS]
- Momcheva, I., Williams, K., Keeton, C., & Zabludoff, A. 2006, ApJ, 641, 169 [ADS]
- Mörtsell, E. & Sunesson, C. 2006, Journal of Cosmology and Astro-Particle Physics, 1, 12 [ADS]
- Moustakas, L. A., Abazajian, K., Benson, A., Bolton, A. S., Bullock, J. S., Chen, J., Cheng, E., Coe, D., et al. 2009, ArXiv e-prints [ADS]
- Moustakas, L. A., Bolton, A. J., Booth, J. T., Bullock, J. S., Cheng, E., Coe, D., Fassnacht, C. D., Gorjian, V., et al. 2008, in Society of Photo-Optical Instrumentation Engineers (SPIE) Conference Series, Vol. 7010, Society of Photo-Optical Instrumentation Engineers (SPIE) Conference Series [ADS]
- Moustakas, L. A., Marshall, P., Newman, J. A., Coil, A. L., Cooper, M. C., Davis, M., Fassnacht, C. D., Guhathakurta, P., et al. 2007, ApJ, 660, L31 [ADS]
- Myers, S. T., Jackson, N. J., Browne, I. W. A., de Bruyn, A. G., Pearson, T. J., Readhead, A. C. S., Wilkinson, P. N., Biggs, A. D., et al. 2003, MNRAS, 341, 1 [ADS]
- Oguri, M. 2007, ApJ, 660, 1 [ADS]

- Oguri, M., Inada, N., Strauss, M. A., Kochanek, C. S., Richards, G. T., Schneider, D. P., Becker, R. H., Fukugita, M., et al. 2008, *AJ*, 135, 512 [ADS]
- Oguri, M., Keeton, C. R., & Dalal, N. 2005, *MNRAS*, 364, 1451 [ADS]
- Olling, R. P. 2007, *MNRAS*, 378, 1385 [ADS]
- Paczynski, B. & Gorski, K. 1981, *ApJ*, 248, L101 [ADS]
- Perlmutter, S., Aldering, G., Goldhaber, G., Knop, R. A., Nugent, P., Castro, P. G., Deustua, S., Fabbro, S., et al. 1999, *ApJ*, 517, 565 [ADS]
- Refsdal, S. 1964, *MNRAS*, 128, 307 [ADS]
- Richards, G. T., Myers, A. D., Gray, A. G., Riegel, R. N., Nichol, R. C., Brunner, R. J., Szalay, A. S., Schneider, D. P., et al. 2009, *ApJS*, 180, 67 [ADS]
- Riess, A. G., Filippenko, A. V., Challis, P., Clocchiatti, A., Diercks, A., Garnavich, P. M., Gilliland, R. L., Hogan, C. J., et al. 1998, *AJ*, 116, 1009 [ADS]
- Riess, A. G., Macri, L., Casertano, S., Sosey, M., Lampeitl, H., Ferguson, H. C., Filippenko, A. V., Jha, S. W., et al. 2009, *ApJ*, 699, 539 [ADS]
- Saha, P., Coles, J., Macciò, A. V., & Williams, L. L. R. 2006, *ApJ*, 650, L17 [ADS]
- Schmidt, S., Newman, J., Tyson, J., Connolly, A., Wittman, D., Matthews, D., Margoniner, V., Choi, A., et al. 2009, in *Bulletin of the American Astronomical Society*, Vol. 41, Bulletin of the American Astronomical Society, 368–+ [ADS]
- Suyu, S. H., Marshall, P. J., Auger, M. W., Hilbert, S., Blandford, R. D., Koopmans, L. V. E., Fassnacht, C. D., & Treu, T. 2009a, *ArXiv e-prints* [ADS]
- Suyu, S. H., Marshall, P. J., Blandford, R. D., Fassnacht, C. D., Koopmans, L. V. E., McKean, J. P., & Treu, T. 2009b, *ApJ*, 691, 277 [ADS]
- van de Ven, G., Mandelbaum, R., & Keeton, C. R. 2009, *MNRAS*, 398, 607 [ADS]
- Yamamoto, K., Kadoya, Y., Murata, T., & Futamase, T. 2001, *Progress of Theoretical Physics*, 106, 917 [ADS]